NAVAL POSTGRADUATE SCHOOL

MONTEREY, CALIFORNIA

THESIS

STUDY OF COMPOSITE MATERIAL FAILURE UNDER TENSILE AND CYCLIC LOADING

by

Carlos J. Diaz-Colon

March 2022

Thesis Advisor: Young W. Kwon
Second Reader: Jarema M. Didoszak

THIS PAGE INTENTIONALLY LEFT BLANK

REPORT DOCUMENTATION PAGE			*Form Approved OMB No. 0704-0188*

1. AGENCY USE ONLY *(Leave blank)*	**2. REPORT DATE** March 2022	**3. REPORT TYPE AND DATES COVERED** Master's thesis

4. TITLE AND SUBTITLE STUDY OF COMPOSITE MATERIAL FAILURE UNDER TENSILE AND CYCLIC LOADING	**5. FUNDING NUMBERS**
6. AUTHOR(S) Carlos J. Diaz-Colon	
7. PERFORMING ORGANIZATION NAME(S) AND ADDRESS(ES) Naval Postgraduate School Monterey, CA 93943-5000	**8. PERFORMING ORGANIZATION REPORT NUMBER**
9. SPONSORING / MONITORING AGENCY NAME(S) AND ADDRESS(ES) N/A	**10. SPONSORING / MONITORING AGENCY REPORT NUMBER**

11. SUPPLEMENTARY NOTES The views expressed in this thesis are those of the author and do not reflect the official policy or position of the Department of Defense or the U.S. Government.

12a. DISTRIBUTION / AVAILABILITY STATEMENT Approved for public release. Distribution is unlimited.	**12b. DISTRIBUTION CODE** A

13. ABSTRACT (maximum 200 words)

Composite structures continue to gain popularity in engineering applications as they offer great strength to weight ratios, design flexibility and can last a long time. However, they are not exempt from catastrophic failure and fail without warning. Unlike metals, composites do not have defined endurance limits or established S-N curves, and their failure mechanism under cyclic loading is still largely underdeveloped. This thesis aimed to use a multiscale approach to predict the residual strength of glass fiber composites (GFC) after cyclic loading, create an S-N curve for GFC and glass fiber bundles (GFB) and assess recently proposed universal failure criteria for notched specimens. GFC and GFB specimens' behavior were analyzed under tensile and cyclic loading. Polymethyl methacrylate (PMMA) and laminated carbon fiber composites (CFC) with cross-ply (CP) and quasi-isotropic (QI) orientations containing various notch shapes were tensile tested and analyzed in Ansys. As a result, a probabilistic model for residual strength after cyclic loading for GFC was created and agreed with the experimental data. Additionally, S-N curves were generated for GFC and GFB. The results of the proposed failure criteria also agreed very well against experimental data for the materials tested with various notch types.

14. SUBJECT TERMS cyclic loading, glass fiber, fiber composites, fatigue failure	**15. NUMBER OF PAGES** 69
	16. PRICE CODE

17. SECURITY CLASSIFICATION OF REPORT	**18. SECURITY CLASSIFICATION OF THIS PAGE**	**19. SECURITY CLASSIFICATION OF ABSTRACT**	**20. LIMITATION OF ABSTRACT**
Unclassified	Unclassified	Unclassified	UU

NSN 7540-01-280-5500

Standard Form 298 (Rev. 2-89)
Prescribed by ANSI Std. 239-18

THIS PAGE INTENTIONALLY LEFT BLANK

Approved for public release. Distribution is unlimited.

STUDY OF COMPOSITE MATERIAL FAILURE UNDER TENSILE AND CYCLIC LOADING

Carlos J. Diaz-Colon
Lieutenant, United States Coast Guard
BS, Excelsior College, 2012

Submitted in partial fulfillment of the
requirements for the degree of

MASTER OF SCIENCE IN MECHANICAL ENGINEERING

from the

NAVAL POSTGRADUATE SCHOOL
March 2022

Approved by: Young W. Kwon
Advisor

Jarema M. Didoszak
Second Reader

Garth V. Hobson
Chair, Department of Mechanical and Aerospace Engineering

THIS PAGE INTENTIONALLY LEFT BLANK

ABSTRACT

Composite structures continue to gain popularity in engineering applications as they offer great strength to weight ratios, design flexibility, and can last a long time. However, they are not exempt from catastrophic failure and fail without warning. Unlike metals, composites do not have defined endurance limits or established S-N curves, and their failure mechanism under cyclic loading is still largely underdeveloped. This thesis aimed to use a multiscale approach to predict the residual strength of glass fiber composites (GFC) after cyclic loading, create an S-N curve for GFC and glass fiber bundles (GFB) and assess recently proposed universal failure criteria for notched specimens. GFC and GFB specimens' behavior were analyzed under tensile and cyclic loading. Polymethyl methacrylate (PMMA) and laminated carbon fiber composites (CFC) with cross-ply (CP) and quasi-isotropic (QI) orientations containing various notch shapes were tensile tested and analyzed in Ansys. As a result, a probabilistic model for residual strength after cyclic loading for GFC was created and agreed with the experimental data. Additionally, S-N curves were generated for GFC and GFB. The results of the proposed failure criteria also agreed very well against experimental data for the materials tested with various notch types.

THIS PAGE INTENTIONALLY LEFT BLANK

TABLE OF CONTENTS

LIST OF FIGURES

THIS PAGE INTENTIONALLY LEFT BLANK

LIST OF TABLES

THIS PAGE INTENTIONALLY LEFT BLANK

LIST OF ACRONYMS AND ABBREVIATIONS

ASTM	American Society for Testing and Materials
CFC	carbon fiber composite
FEM	finite element method
GFB	glass fiber bundle
GFC	glass fiber composite
MATLAB	matrix laboratory
MTS	Material Testing System
NPS	Naval Postgraduate School
PMMA	polymethyl methacrylate

THIS PAGE INTENTIONALLY LEFT BLANK

ACKNOWLEDGMENTS

I am truly thankful for everyone that took the time to support, encourage, and guide me throughout this process! It took a village, and I share this incredible achievement with you. First and foremost, I would like to thank my previous supervisors and mentors, CAPT Eric Carrero, CAPT Janet Espino-Young, and CDR Jose Rosario (NPS alum). Your leadership and guidance pushed me to be a better officer and ultimately led to my selection into the Coast Guard's Advanced Education program. To Dr. Kwon, my thesis advisor and graduate school "compass," thank you for keeping me focused and settling my thoughts. It felt like I was always stressing about something before our weekly meetings; however, I would leave feeling like I could do anything after talking with you. To Dr. Didoszak, thank you for your patience, support, and perspective on the thesis process; this too shall pass. To Dr. Park and John Mobley, thank you for your assistance in preparing and testing my samples; even on short notice, you were always available and willing to support me. To the Mechanical Engineering department, thank you! You took a liberal arts major and turned him into a mechanical engineer. I am incredibly grateful for all of you; however, I wanted to thank a few professors that stood out; Professor Adams, Dr. Gordis, Dr. Bingham, Dr. Dausen, Dr. Ansell, Dr. Austin (math department), and of course, Dr. Kwon. To my cohort and peers I met along the way, thank you. Sharing the academic struggles and working together to figure them out is an experience I will never forget.

To my beautiful wife, Ariannis, and boys, Jonathan, Carlos, Benjamin, and Emilio. Thank you for your support and understanding. You sacrificed a lot of nights and weekends so that I could study and or try to understand a new concept. You guys are the reason I strive to be a better version of myself; I would have absolutely not been able to complete this without any of you.

THIS PAGE INTENTIONALLY LEFT BLANK

I. INTRODUCTION

A. BACKGROUND

The increased use of composite structures in civil, aerospace, and mechanical engineering applications motivates a greater understanding of their behavior under repeated stress. Typical examples range from fiber-reinforced concrete used in construction, to fiber-reinforced composites in aircraft and automotive industries, to glass or carbon fiber composites used in vessel design [1-2]. Composite structures are also becoming increasingly popular in military applications due to their high strength-to-weight ratio [3]. While usage differs in many of these applications, all are vulnerable to repeated stress caused by vibration or cyclic loads, which leads to fatigue and eventual material failure. Though composite structures have been around for several decades, there is still a great deal to learn about their residual strength after being subjected to cyclic loading.

Moreover, the ability to determine the service life of a composite structure before a catastrophic failure is still largely underdeveloped. In their research of unidirectional glass fiber reinforced composites, Zangenberg et al. [4]. concluded, "Despite the fact that unidirectional fiber reinforced composites is the simplest kind of laminated materials, the fatigue failure mechanisms are complicated and not understood in detail." As use of composite structures surges in engineering applications, prediction of fatigue failure, and service life predictions, must improve. A probabilistic model for residual strength as a function of cyclic load is introduced for glass fiber composite (GFC). This thesis aims to correlate the behavior and fatigue failure of GFC to the behavior and fatigue failure of dry glass fiber bundles (GFB).

In addition to fatigue failure analysis, recently proposed failure criteria for brittle notched material were evaluated. In [5], Kwon suggests universal failure criteria apply to any load-carrying application regardless of whether the materials have a notch, crack, or neither. The theory discussed in [5] states that two conditions must be met for failure to occur. First, "the local stress must not be lower than the failure strength of the material," while the second condition states that the stress-gradient criterion must be satisfied.

The following subsections provide an overview of composite structures and their general makeup and discuss the current failure theories for cracks and notches. The current state-of-the-art for failure analysis after cyclic loading and the proposed failure criteria are provided in Chapter II, followed by experimental procedures and numerical analysis in Chapters III and IV, respectively. Finally, the results and conclusions are provided in Chapters V and VI.

1. Composite Structures

A typical composite structure is artificially made of two bonded materials, in which a stiff and robust material is used to strengthen a weak and softer one [6-8]. The weaker material is the matrix or binding material, while the former is called the dispersed phase or reinforcing material. The dispersed phase and focus of the first part of this research is glass fiber with unidirectional (UD) long-fiber concentration distribution. In other words, the glass fibers are bundled and continuous in one direction inside the matrix.

This setup, however, is only one of the many different variations of a composite structure. The reinforcement materials may be short, long, or woven and made of carbon, glass, Kevlar, or graphite, to list a few, with aligned or randomly oriented materials inside the matrix. Matrix variation is no different. Composite matrix materials are vast and include polymer, metal, ceramic, cement, and others. Callister and Rethwisch [6] classified composites into four main categories: particle-reinforced, fiber-reinforced, structural, and Nano. In this thesis, fiber-reinforced and structural composites are analyzed. Figure 1 shows a general schematic of a typical fiber-reinforced composite.

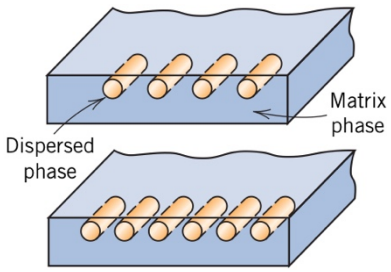

Figure 1. Composite schematic showing matrix/dispersed relationship with a continuous UD reinforcement in an isotropic matrix. Adapted from [6].

Structural composites are multi-layered and are most commonly made up of laminar composites or sandwich panels. Laminar composites have two-dimensional sheets bonded together and are continuous throughout the plies. The multi-layered structure can be configured as UD, cross-ply (CP), angle-ply (AP), and multidirectional (MD), as seen in Figure 2. The laminar properties will change with each configuration. Sandwich composites are a more robust top and bottom layer with a weaker core "sandwiched" in-between, similar to a cardboard box with a corrugated or honeycomb center.

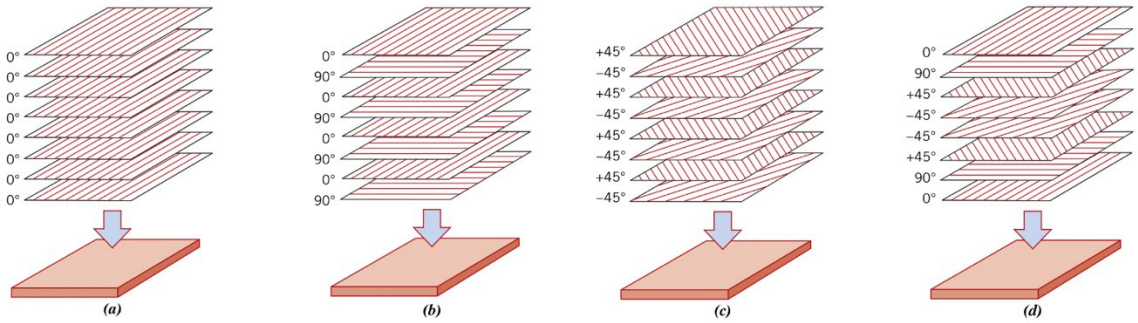

Figure 2. Lay-up for laminar composites. (a) Unidirectional; (b) cross-ply; (c) angle-ply; and (d) multidirectional. Adapted from [6].

There are many variations in the composite structure makeup, which makes developing an acceptable failure method challenging [7]. As a result, residual strength modeling after cyclic loading is underdeveloped or made with inaccurate assumption. This thesis takes a multiscale approach to analyze a glass fiber composite in its simplest form: UD fibers in an isotropic matrix. The behavior of the composite after cyclic loading will be compared to its dry fiber bundle to establish a relationship and mathematical model for residual strength after cyclic loading. Once a reliable model is developed for a glass fiber composite, the same model may be applied to other composite structures such as carbon fiber or boron fiber. Further, this model can assist with designing a specified service life for fibrous composite structures.

2. Failure Criteria for Crack and Notch Deformations

The study and analysis of fracture mechanics began to gain attention when fractures in high-strength materials were noted on systems with relatively low operating stress [9]. Since the inception of fracture mechanics in the early 1900, several theories have been developed and widely accepted to accurately calculate crack propagation due to fatigue. In general, there are two main categories for fractures mechanics: ductile and brittle. A brittle fracture tends to happen rapidly, without warning and is the focus of the second part of this research.

Modern theories of fracture mechanics can be traced back to Griffith's fracture theory in 1921 and Irwin's stress intensity factors in 1957. Griffith's theory provided a mathematical framework based on energy balance wherein work is done to extend or grow the crack, and Irwin proposed stress intensity factor, K, that can express stresses around a crack for each loading mode [6], [8], [9]. Based on these theories, linear fracture mechanics were determined for line cracks, while notch theories followed global or local criteria. The recently proposed failure criteria [5] would eliminate the need to go back and forth between theories and determine the failure location and path. Should the theory hold, it can unify fracture mechanics' crack propagation and several notch theories.

B. OBJECTIVE

This thesis aims to use a multiscale approach to predict fatigue failure of fibrous composite materials and structures with the following objectives:

1. Predict residual strength after cyclic loading for any number of cycles.
2. Create an S-N curve for glass fiber composites and glass fiber bundles.

In addition, this thesis will further assess a universal failure criteria for a notched specimen. To this end, the last objective is to test the new theory against experimental data.

II. STATE OF THE ART

A. FATIGUE FAILURE AFTER CYCLIC LOADING

A literature review was conducted to understand the current state of the art in determining a glass fiber composite's fatigue life or residual strength after cyclic loading. However, there was a limited amount of research devoted specifically to UD glass fiber composites, the focus of this study. Therefore, prediction methods for all composite materials are briefly discussed, as they also apply to UD glass fiber composites.

1. Fatigue Failure: Why Do We Care?

The degradation of material properties due to fluctuating loads over time is called fatigue, and the resulting failure is called fatigue failure [7]. Fatigue failure is one of the most common reasons materials fail in modern engineering applications and accounts for approximately ninety percent (90%) of all failures in metals; composite structures are also susceptible to fatigue failure [6], [8]. Failure at the maximum load is not as common as fatigue failure in most applications, primarily due to knowledge of the material properties and engineering constraints when designing the application. Instead, failure occurs when the material is subjected to repeated or fluctuating stresses or strain, often below the material's yielding strength. In other words, if the application is being used as designed, material failure comes from fatigue rather than from reaching the material's ultimate strength.

Fatigue analysis, however, is not a new concept, as the first study of metal fatigue is believed to have been conducted around 1829 [7]. Since then, many scientists and engineers have contributed a great deal of research, analysis, and mathematical modeling to better understand fatigue failure across a variety of materials, metallic and nonmetallic. Unfortunately, despite all the advances made in fatigue analysis, composite structures continue to challenge modern designs. Numerous fatigue theories and mathematical models have been developed to predict better fatigue failure of fiber composite structures subjected to cyclic loading; however, none are as accurate as their isotropic counterparts,

specifically metals. Simply put, fatigue failure models for fiber composite structures are still underdeveloped.

2. Fatigue Life or Residual Strength Modeling and Prediction Methods

Many fatigue life or residual strength models and prediction methods used for composite structures were developed through experimental programs wherein empirical data was collected [7]. These theories typically followed two methodologies to describe the composite failure: phenomenological or microscale analysis.

A phenomenological model uses empirical relationships at the macro level and is consistent with fundamental laws of mechanics with defined variables and parameters [10-17]. These models were beneficial in understanding the general behavior of the composites and their failure modes; however, they required certain assumptions. In [11], Philippidis et al. analyzed theory vs. experimental data for several widely accepted macroscale residual strength models. They concluded, "some models are able to describe in several cases the phenomenon of strength degradation, while others fail to provide consistently a good prediction of this behavior." Furthermore, they were unable to find a macro model that was 100% reliable when varying the loading conditions.

The microscale approach assumes homogeneous or normalization to examine the macro behavior based on micro information [18], [19]. This method uses analytical or numerical analysis to interpret the constitutive relationship and can replace expensive physical testing [20-25]. However, as noted by Srilakshmi et al. [18], one of the main disadvantages of these models is that they are "inefficient in modelling and numerical computation difficulties arise." One example of this problem is seen in [23], wherein the progressive damage approach "could not accurately follow the progression of the failure" in one of their tested specimens. In addition, Hosseiny and Jakobsen [23] found that the delamination length is underestimated; however, they suggested that a more refined, expensive mesh may improve the estimation.

A relatively new approach to analyzing the residual strength of a composite structure is the multiscale approach. Here, the material properties are linked between the microscale and macroscale to help determine stresses and strains at the constituent and

composite structure levels, respectively [26-29]. This new approach attempts to bridge the macroscale and microscale together to produce more accurate results and is the basis for the analysis of the glass fiber composite in this paper.

B. UNIFIED FAILURE CRITERIA OF BRITTLE NOTCHED MATERIAL

As proposed in Kwon [5], the new failure criteria have the potential to predict failure location and direction. This theory is based on the following criteria expressed in equations (1) and (2).

$$\sigma_l \geq \sigma_f \tag{1}$$

$$\frac{\sigma^3}{2E}\left|\frac{d\sigma}{ds}\right|^{-1} \geq \kappa_{fail} \tag{2}$$

In equation (1), the local stress σ_l from the applied load must be greater than or equal to the tensile strength or failure stress σ_f of the brittle material. This criterion is based on the Maximum-Normal stress theory for axial loading and provides a potential failure location. In equation (2), a stress gradient condition is given $\left|\frac{d\sigma}{ds}\right|^{-1}$ to determine the failure direction where s is along the failure's path. Here, κ_{fail} is a critical value assumed to be the material constant and is determined during the initial tensile test for the notched specimen; E is Young's modulus. When the left side of equation (2) is at a maximum in one direction at the local stress σ_l, the location of that maximum is the failure direction. Thus, failure location and direction for a notched or unnotched specimen will occur when both criteria in equations (1) and (2) are met.

Equation (2) is further evaluated in [5] to determine the relationship of the failure stress on an infinite plate with a circular hole of radius R under tension. The normal stress around the hole is expressed in equation (3), where r is the radial distance from the center of the hole, perpendicular to the applied load. Taking a derivative in terms of the stress gradient along the vertical direction and substituting it into equation (2) yields the relationship between failure stress and the hole radius, as seen in equation (4). Kwon

concludes that the failure stress is inversely proportional to one-third power of the radius of a hole on an infinite plate [5].

$$\sigma = \frac{1}{2}\left[\left(1+\frac{R^2}{r^2}\right)+\left(1+\frac{3R^4}{r^4}\right)\right] \tag{3}$$

$$\sigma \propto R^{-1/3} \tag{4}$$

III. EXPERIMENTAL PROCEDURES

A. SPECIMEN DESCRIPTION

1. Glass Fiber: Composites and Dry Bundles

The GFC tested in this study came from a prefabricated, 0° UD, glass/epoxy laminate plate, with glass fibers oriented vertically along the y-axis. The plate had a nominal thickness of 1.4 mm and was cut with a water jet to rectangular specimens of 70 mm x 10 mm at the NPS machine shop. Aluminum tabs were then attached with a two-part epoxy on both ends to avoid premature failure at the grips during tensile and cyclic testing. Figure 3 shows the GFC dimensions; aluminum tabs are colored light blue, and glass fibers are gray.

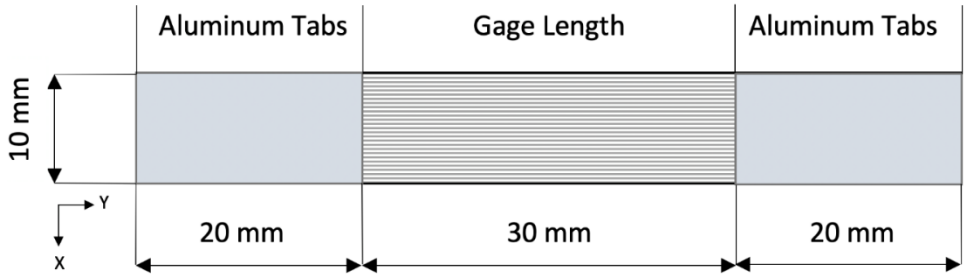

Figure 3. GFC Dimensions with fibers parallel the y-axis.

Commercially available E-glass fiber bundles were taken from a roll of UD fabric, model number TG-13-U, made by TEXONIC [30]. The fiber bundles were cut to 565 mm and had an average width and thickness of 3 mm and 0.5 mm. Similar to the dry carbon fibers in [27], these dry glass fibers were tangled and intertwined inside the fiber bundle, which also caused some slack between individual fibers resulting in an uneven stress distribution for tensile and cyclic testing. Figures 4 and 5 show magnified views of the tangled fibers taken with scanning electron microscopy (SEM) at 30X and 430X, respectively. Their behavior under tensile and cyclic loading is discussed in the results chapter.

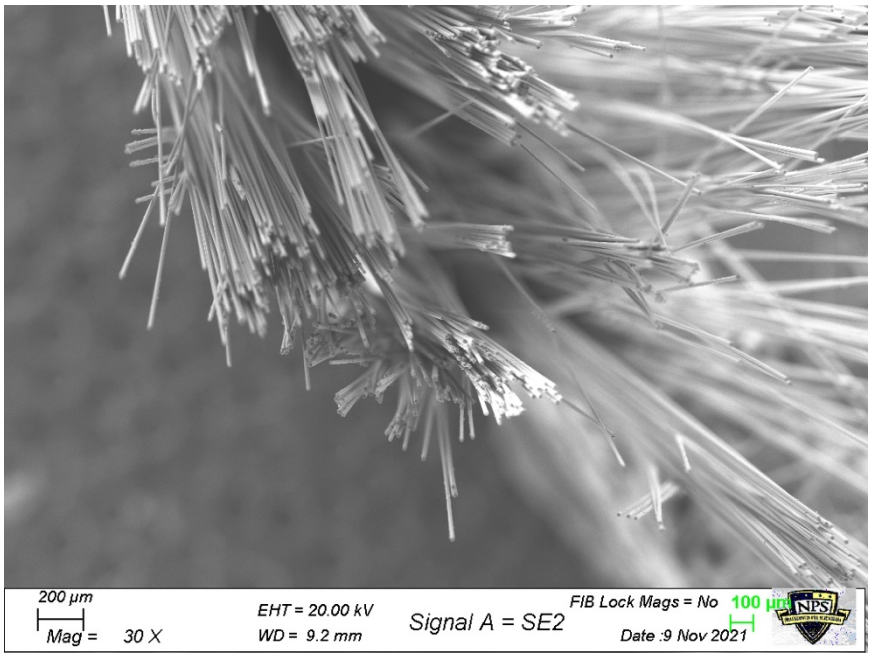

Figure 4. Glass fiber orientation inside a dry fiber bundle taken at 30X magnification.

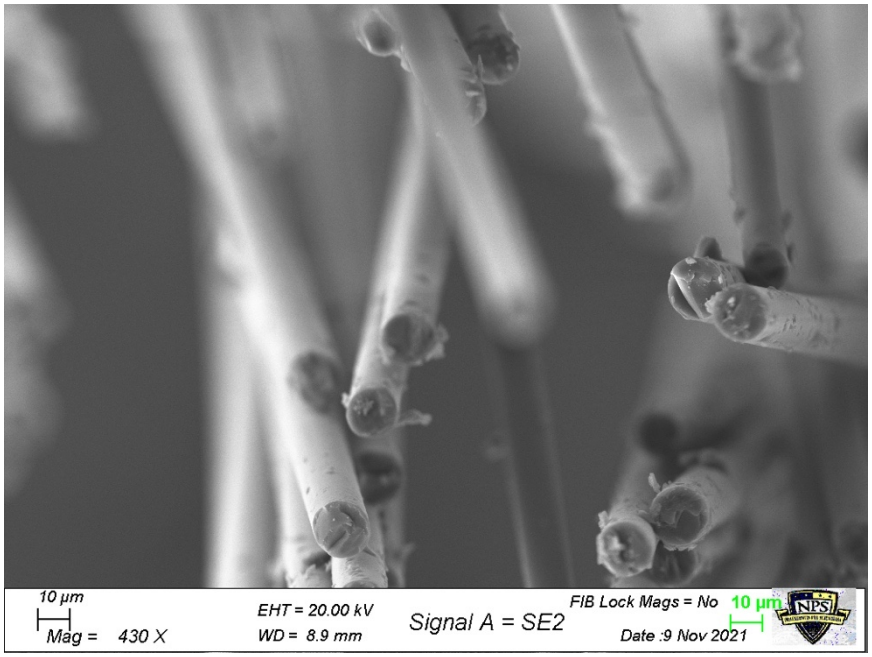

Figure 5. Glass fiber orientation inside a dry fiber bundle taken at 430X magnification.

2. Brittle Materials

Polymethyl methacrylate (PMMA) and laminated CFC Quasi-Isotropic (QI) and Cross-Ply (CP) specimens used in this study measured 140 mm x 24 mm and had a nominal thickness of 6 mm and 1.4 mm, respectively. The two sets of laminated CFC were composed of several plies bonded in QI and CP orientations, as described in Figures 2 (b) and (d). Gage lengths for PMMA and CFC specimens were set to 100 mm, leaving 20 mm at both ends for grip placement in the test equipment. Material properties for PMMA were determined by conducting a tensile test with two 90° degree strain gages attached to the center of a dog-bone-shaped design. Properties for CFC QI and CP specimens were previously determined and provided for this research.

The PMMA and CFC specimens had various notch shapes made at the specimen's midpoint using a water jet. The machined perorations consisted of circular holes with various diameters, 4 mm and 6 mm horizontal cracks with various angles, an elliptical hole, and one specimen containing evenly spaced double circular holes along the x-axis.

B. MECHANICAL TESTING

In this study, an Instron 5982 [31] and MTS 858 Table Top System [32] were used to investigate material failure. The Instron is a screw-driven testing system with a 100 kN maximum force capacity, and the MTS is a hydraulic testing system with a 10 kN maximum force capacity. A low strain rate of 2 mm/min was used for the tensile test, and a loading rate of 0.5 Hz with 16 data points per second was used for cyclic loading.

Equipment selection was based on the expected failure of the specimen or the equipment's capability. Both systems meet ASTM testing requirements for tension and compression; however, only the MTS could conduct cyclic loading. Figure 6 shows standard images for the Instron and MTS testing systems used in this study.

Figure 6. Standard images for the testing systems used in this study. Left: INSTRON 5982. Source: [31]. Right: MTS 858 Table Top System. Source: [32].

1. Tensile Test

A minimum of three specimens per material and notch type were measured, and tensile tested to failure to establish their respective baseline tensile strengths. In addition to the baseline strengths, linear strain gages were attached to several dog-bone-shaped GFC and PMMA samples to establish Young's Modulus and Poisson's Ratio, as seen in Figure 7. The Instron was used for the GFC, PMMA, and CFC specimens, as their maximum tensile strengths were higher than the MTS 10 kN capacity. The GFB was tested with the MTS.

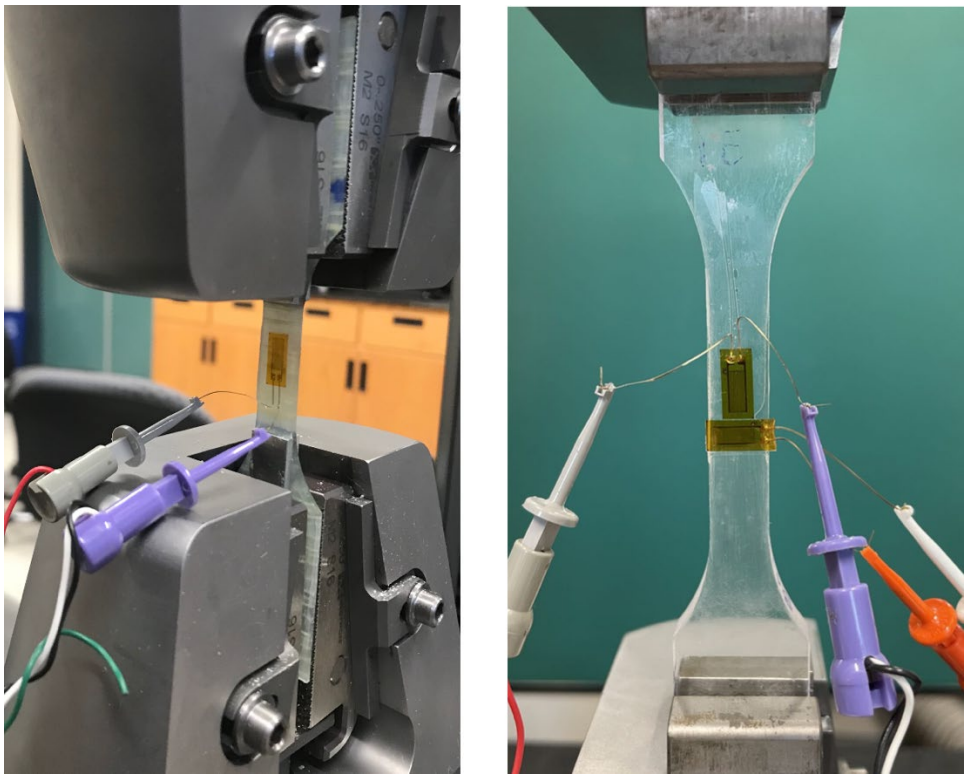

Figure 7. Dog-bone-shaped GFC (left) and PMMA (right) with strain gages attached.

Test setup and grip placement were standard for GFC, PMMA, and CFC specimens; however, an adapter was required to test the fiber bundles. The GFB was prepared and tensile tested with the MTS using an indirect grip technique described in [27]. As previously mentioned, the fiber bundles were pre-cut to 565 mm, then evenly wrapped 2.25 (2 1/4) times around two cylindrical adapters until reaching an approximate gauge length of 79 mm. This technique was adopted from previous thesis research conducted at NPS to remain consistent with dry fiber bundle testing [3]. Figure 8 shows GFB wrapped around the cylindrical adapters; before and after being gripped by the MTS. This setup was identical for both tensile and cyclic testing.

Figure 8. GFB wrapped around the cylindrical adapter before (left) and after (right) being gripped.

2. Cyclic Testing

Tension-tension axial stress was applied to GFC and GFB specimens at a predetermined load based on their respective tensile strength with a stress ratio, $\bar{R}$, equal to 0.1 (e.g., minimum stress divided by maximum stress). Specimens were either tested to failure or tested to a specified number of cycles, and then tensile tested to failure. The latter was used to determine the specimen's residual strength. The initial test parameters varied in maximum stress, σ_{max}, minimum stress, σ_{min}, mean stress, σ_m, and amplitude stress, σ_a until an optimal value was found. For this study, the optimal stress value was a value that allowed cyclic loads to fail after six thousand (6,000) cycles or about 4 hours. Cyclic tests were force-controlled with maximum and minimum stress assigned. Mean stress and amplitude stress were equated using equations (5) and (6), respectively.

$$\sigma_m = \frac{\sigma_{max}+\sigma_{min}}{2} \quad (5)$$

$$\sigma_a = \frac{\sigma_{max} - \sigma_{min}}{2} \quad (6)$$

a. GFC

Various stress amplitudes were tested to find an optimal stress value where the GFC would fail in a range of four to five hours and just after reaching six thousand (6,000) cycles. The optimal stress value was found to be 5,333 MPa after testing at 1,333 MPa, which did not fail after 19 hours, and 6,000 MPa, which failed quickly after 44 cycles. Then after finding the optimal stress, GFC underwent cyclic loading at stopped every one-thousand (1,000) cycles until reaching six-thousand (6,000) cycles. Residual strength was then determined by tensile testing each specimen post cyclic loading. Table 1 outlines the test parameters used to find the optimal applied stress and testing parameters to find the residual strength.

Table 1. Cyclic test parameters for GFC.

σ_{max}	σ_{min}	σ_m	σ_a	Desired Cycles
1333 MPa	133 MPa	733 MPa	600 MPa	Until failure
6000 MPa	600 MPa	3300 MPa	2700 MPa	Until failure
5333 MPa	533 MPa	2933 MPa	2400 MPa	Until failure
5333 MPa	533 MPa	2933 MPa	2400 MPa	1000
5333 MPa	533 MPa	2933 MPa	2400 MPa	2000
5333 MPa	533 MPa	2933 MPa	2400 MPa	3000
5333 MPa	533 MPa	2933 MPa	2400 MPa	4000
5333 MPa	533 MPa	2933 MPa	2400 MPa	5000
5333 MPa	533 MPa	2933 MPa	2400 MPa	6000

b. GFB

The GFB was tested under cyclic load until failure at a specified maximum and minimum stress, like the GFC. After finding the average tensile strength for the bundle, 280 MPa, three cyclic tests were conducted until failure at 67%, 50%, 40%, 30%, 20%, and 10% of the tensile strength. Table 2 outlines the cyclic test parameters for the GFB.

Table 2. Cyclic test parameters for GFB.

σ_{max}	σ_{min}	σ_m	σ_a	Desired Cycles
187 MPa	19 MPa	103 MPa	84 MPa	Until failure
140 MPa	14 MPa	77 MPa	63 MPa	Until failure
112 MPa	11 MPa	62 MPa	47 MPa	Until failure
85 MPa	9 MPa	47 MPa	37 MPa	Until failure
56 MPa	6 MPa	31 MPa	24 MPa	Until failure
28 MPa	3 MPa	15 MPa	13 MPa	Until failure

IV. NUMERICAL ANALYSIS

A plane stress finite element method (FEM) model was created in Ansys [33] for PMMA and CFC, QI and CP, specimens to analyze their respective failure location and direction, as proposed in [5]. Material properties resulting from the tensile tests were also created and used in the analysis. Specimen notch type and dimensions are outlined in Tables 3 and 4 for PMMA and CFC, respectively.

A. GEOMETRY

Each specimen's measurements were evaluated at their maximum and minimum values, which varied plus or minus three percent (+/- 3%). An optimal value was used for each model's geometry, as the recorded maximum and minimum values had little to no effect in the analysis. In addition, quarter model representations were used where symmetry could be applied to improve the time to evaluate the solution.

As previously mentioned, notched specimens were created with a waterjet which did not affect the CFC center hole or ellipse designs; Figures 9 and 10 show their respective FEM. However, the waterjet could not create an even slit to represent a notch crack for the PMMA specimens and created a dumbbell-like shape, as seen in Figure 11. Therefore, the same dumbbell shape was created and used in the FEM for all PMMA crack variations. Figure 12 shows a close-up view of the quarter model's dumbbell shape, followed by the quarter model geometries for a 4 mm and 6 mm notch crack seen in Figure 13. Finally, full-size models were created for the angled PMMA specimens P4 through P6 and CFC QI5. A close-up view of the dumbbell shape for the full-size model is shown in Figure 14, followed by the angled PMMA and CFC's double center hole models in Figures 15 and 16, respectively.

Table 3. PMMA FEM notch type and dimensions.

Specimen	Notch Type	Length	Angle	Model type
P2	Crack	4 mm	0°	Quarter model
P3	Crack	6 mm	0°	Quarter model
P4	Crack	6 mm	15°	Full-size model
P5	Crack	6 mm	30°	Full-size model
P6	Crack	6 mm	45°	Full-size model

Table 4. CFC, QI and CP, FEM notch type and dimensions.

Specimen	Notch Type	Diameter	Model type
QI2	Center hole	3 mm	Quarter model
QI3	Center hole	6 mm	Quarter model
QI4	Center hole	8 mm	Quarter model
QI5	Double Center hole	3 mm each	Full-size model
QI6	Ellipse	4 mm x 8 mm	Quarter model
CP1	Center hole	3 mm	Quarter model
CP2	Center hole	6 mm	Quarter model
CP3	Center hole	9 mm	Quarter model

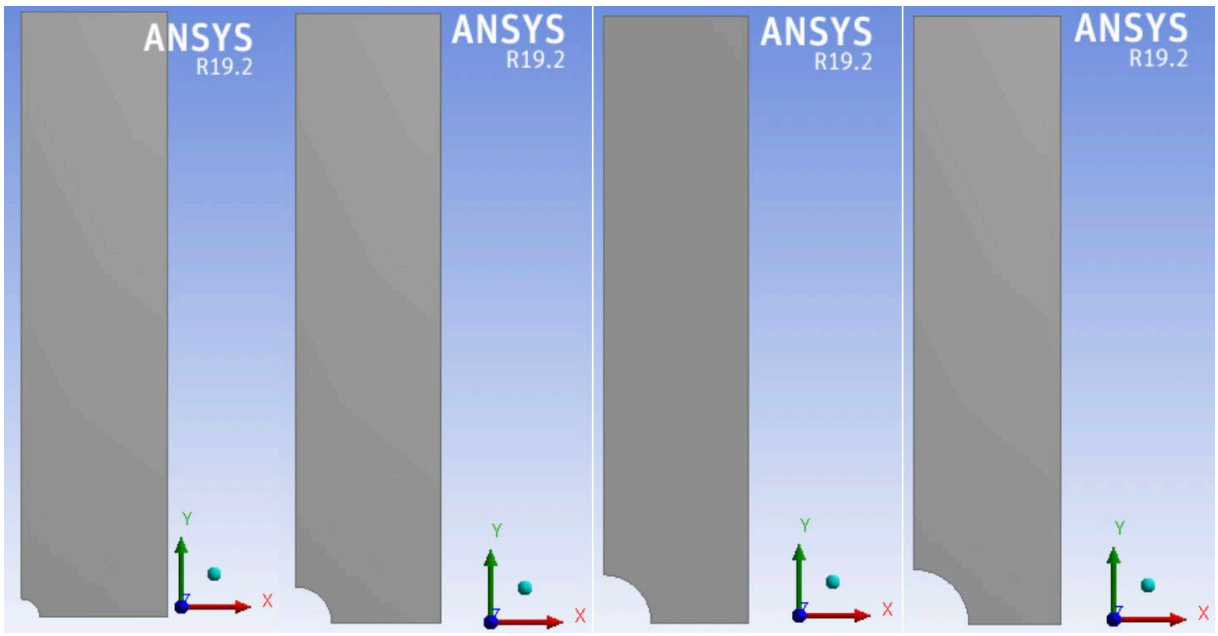

Figure 9. CFC QI and CP center hole geometry. Diameters are 3 mm, 6 mm, 8 mm, and 9 mm from left to right.

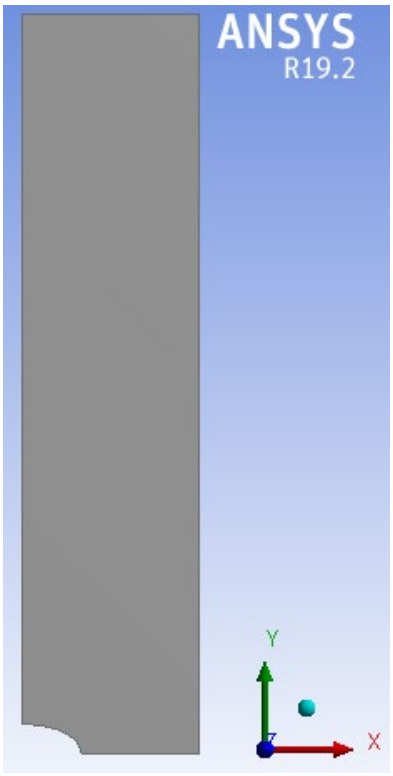

Figure 10. CFC QI6 Ellipse with a 4 mm x 8 mm dimension.

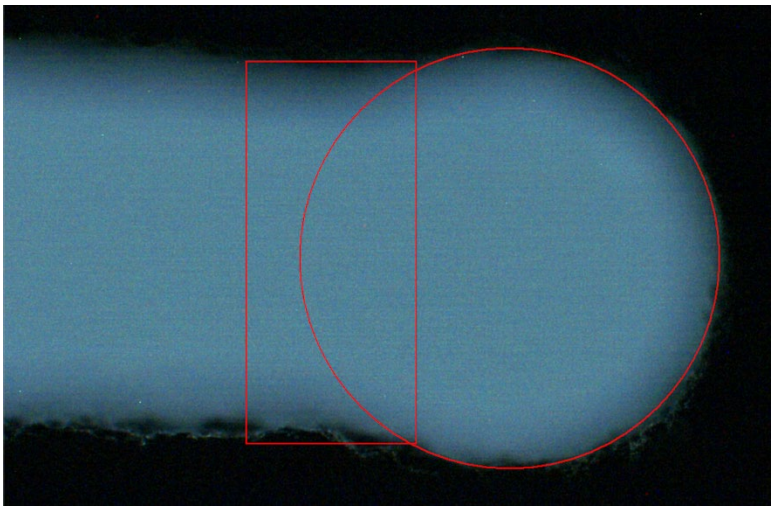

Figure 11. Optical microscopic view of slit created with a waterjet.

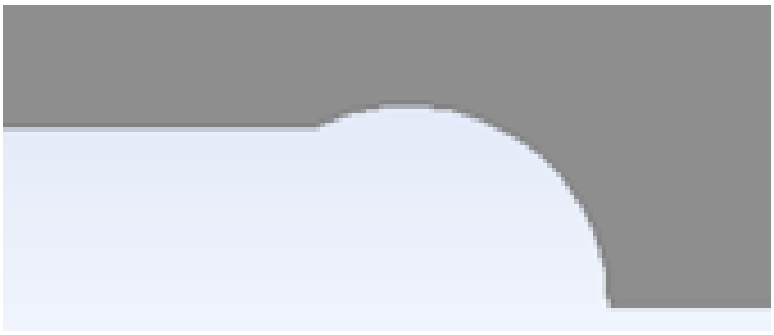

Figure 12. Close-up view of dumbbell shape geometry for the quarter model.

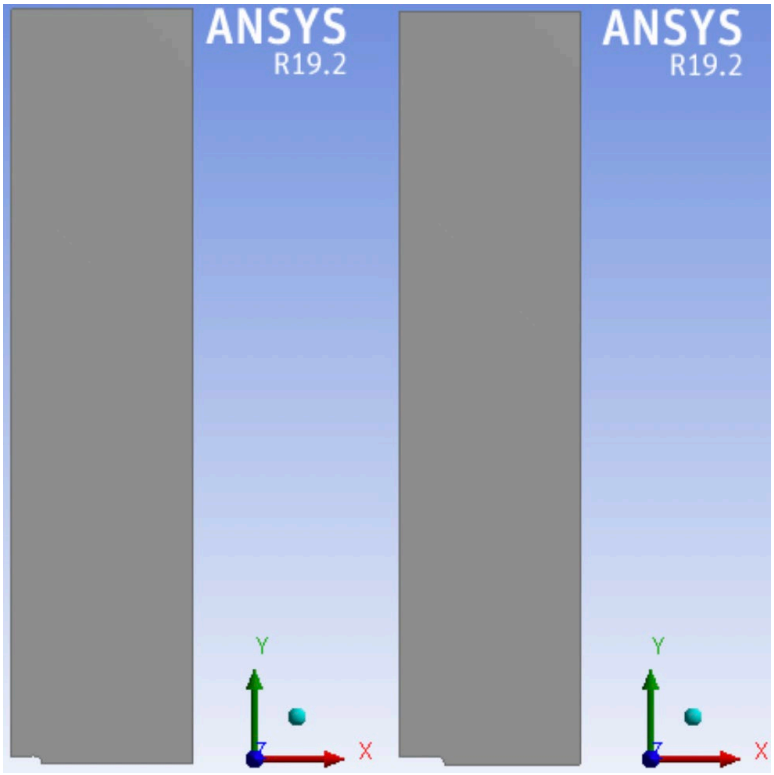

Figure 13. PMMA specimen P2 (left) and P3 (right) with crack lengths of 4 mm and 6 mm, respectively.

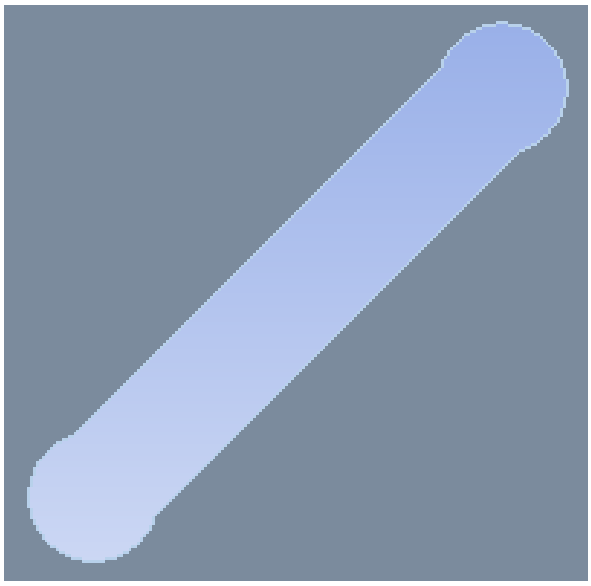

Figure 14. Close-up view of dumbbell shape geometry for the full-size models.

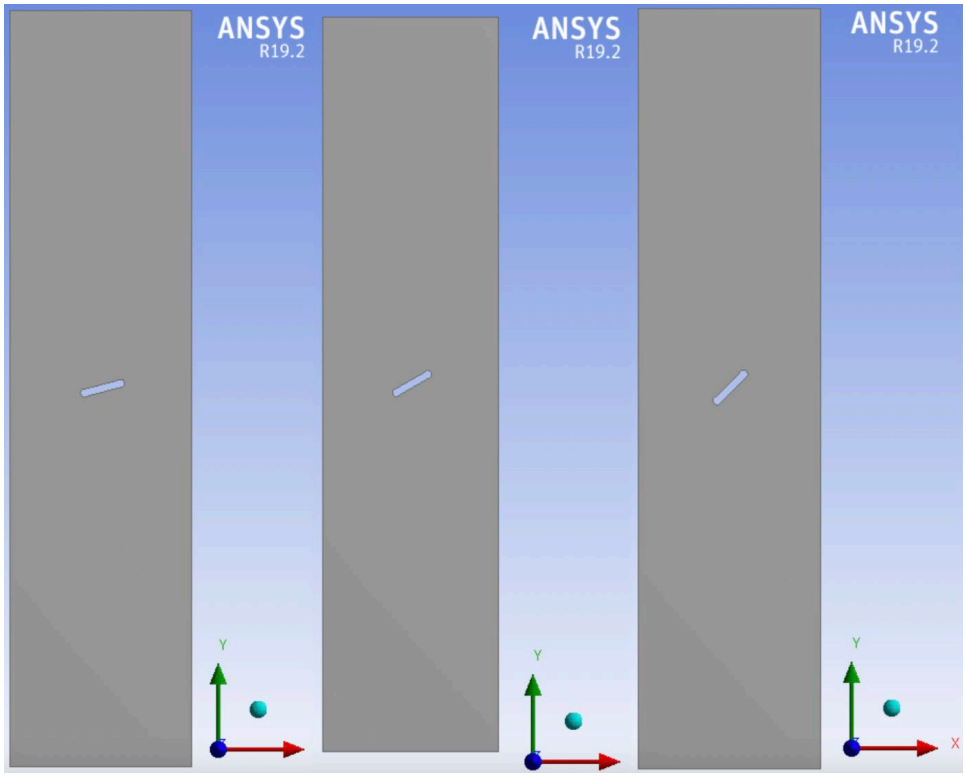

Figure 15. PMMA specimen P4 (left), P5 (center), and P6 (right).

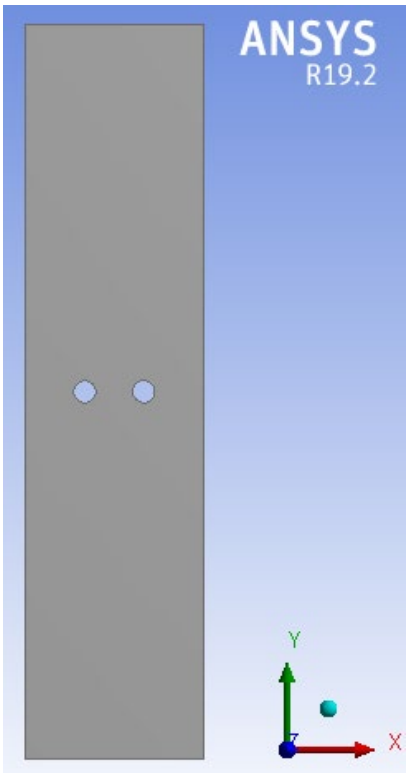

Figure 16. CFC QI5 with two 3 mm diameter holes.

B. DISPLACEMENT AND CONSTRAINTS

A uniform displacement under tension was applied to all models based on their respected tensile test data. PMMA specimens were modeled with a displacement of 0.028 mm, while the CFC QI and CP displacements were modeled with 0.03 mm. Figure 17 shows a quarter model with the displacement location and direction at "C" with vertical and horizontal constraints at "A" and "B," respectively. In Figure 17, the displacement and direction are labeled "B" with fixed support assigned to location "A." Displacement and constraints were set up as described for all quarter and full-sized FEM regardless of notch type.

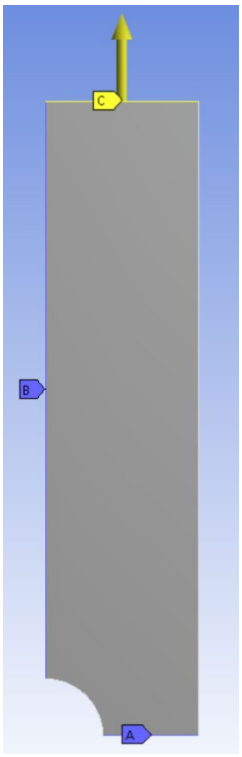

Figure 17. Quarter model with displacement and constraints.

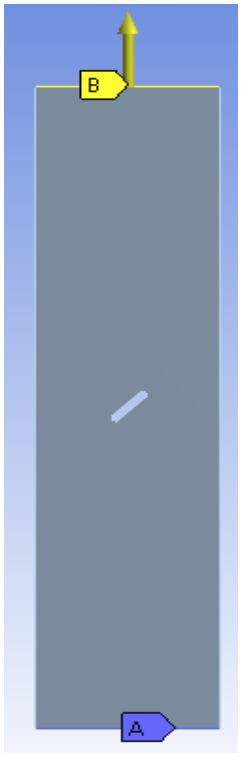

Figure 18. The full-sized model with displacement and constraint.

C. FINITE ELEMENT MESH

All models were meshed using eight-node serendipity elements for the plane stress analysis as seen in Figure 19. A mesh sensitivity analysis was conducted for different element sizes and refinements. An element size of 0.1 mm was selected as the optimal size as it ensured the model was sufficiently meshed for the analysis and the resulting stress values were consistent. Total nodes and elements for each specimen analyzed are outlined in Table 5.

Table 5. Finite element mesh information.

Specimen	Geometry	Element Size	# of Elements	# of Nodes
P2	1/4 model	0.1 mm	59903	180948
P3	1/4 model	0.1 mm	59850	180789
P4	Full-size model	0.1 mm	239408	720822
P5	Full-size model	0.1 mm	239342	720628
P6	Full-size model	0.1 mm	239157	720063
QI2	1/4 model	0.1 mm	59813	180674
QI3	1/4 model	0.1 mm	59542	179831
QI4	1/4 model	0.1 mm	58854	177753
QI5	Full-size model	0.1 mm	238831	719130
QI6	1/4 model	0.1 mm	59428	179489
CP1	1/4 model	0.1 mm	59854	180769
CP2	1/4 model	0.1 mm	59497	179580
CP3	1/4 model	0.1 mm	58644	176991

The location where the maximum stress occurred had to be known to determine the failure location as part of this analysis. Therefore, the FEM was solved for maximum stress. After locating the maximum stress location for each notch type, five elements and six nodes were analyzed along the failure direction to determine the stress gradient for each specimen. Figures 20 and 21 show a representation of the quarter model and the full-size model's mesh, respectively.

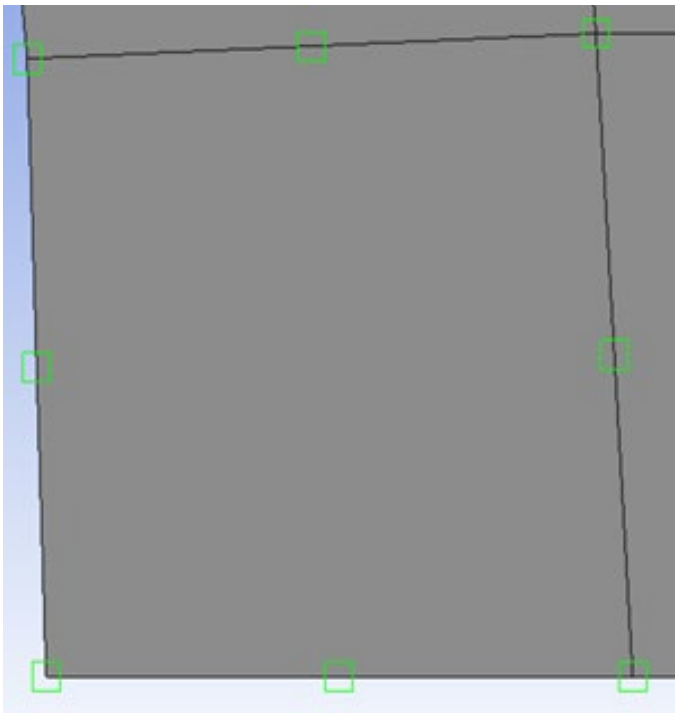

Figure 19. Eight-node serendipity element used for the plane stress analysis.

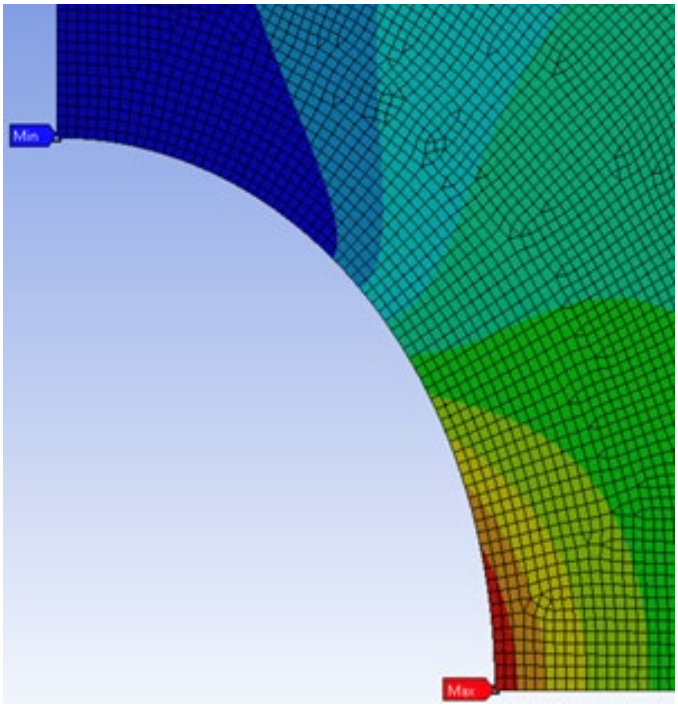

Figure 20. Representation of quarter model's mesh.

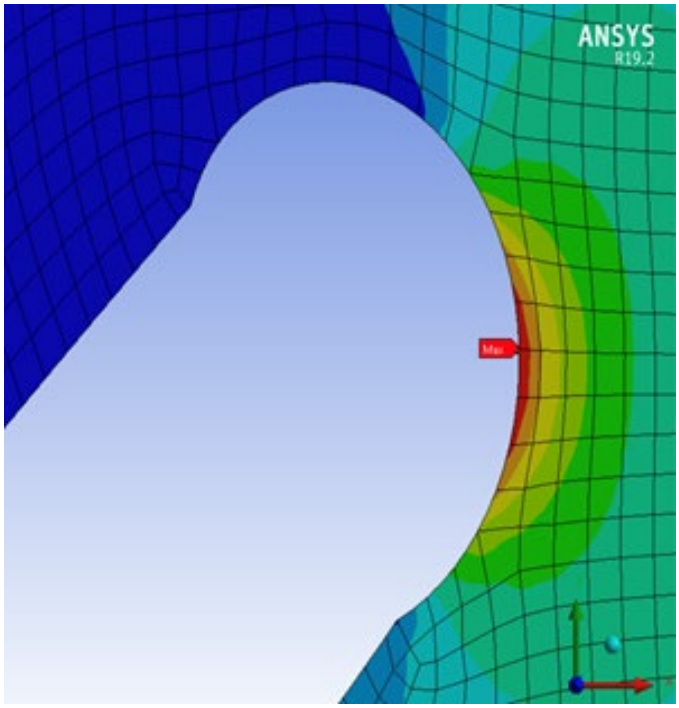

Figure 21. Representation of full-size model's mesh zoomed in at the maximum stress location.

V. RESULTS AND DISCUSSION

A. FATIGUE ANALYSIS

1. Tensile Test

As previously mentioned, three GFC and GFB specimens were tensile tested to establish their respective material properties and analyze their behavior. The average tensile strength and elastic modulus for GFC and GFB are listed in Table 6, with their respective stress and strain curves shown in Figures 22 and 23.

The behavior under tensile stress for GFC and GFB was consistent for each specimen. Both specimen types had an initial nonlinear slope, followed by a linear elastic slope until reaching their respective maximum tensile strength. As mentioned and shown in Figure 5, fiber orientation within the GFB is not linear. It is often tangled or intertwined in various locations along the bundle, causing some slack between fibers. Because of this, fibers are unevenly stressed when subjected to a load which causes premature fiber failure within the bundle. The slack fibers are believed to cause the initial nonlinear slope in the case of the glass fiber bundle. Then when the applied tension removes all slack from the bundle, a linear slope is produced. Similarly, the nonlinear slop of the GFC could represent the behavior of the matrix prior to engaging the embedded fibers. A linear slope is produced once the tension force is high enough to engage the fibers and the matrix.

After reaching their respective maximum tensile strength, the behavior of GFC and GFB are pretty different. In the case of the GFC, failure occurred quickly after reaching its maximum strength, showing a short period of residual strength before an immediate failure. The GFB, on the other hand, displayed a gradual and linear decrease of its residual strength until complete failure.

Table 6. Average tensile strengths for GFC and GFB.

Material	Maximum Force Applied	Tensile Strength	Elastic Modulus
GFC	12,500 (N)	862 (MPa)	5871 (MPa)
GFB	420 (N)	280 (MPa)	3.6 (MPa)

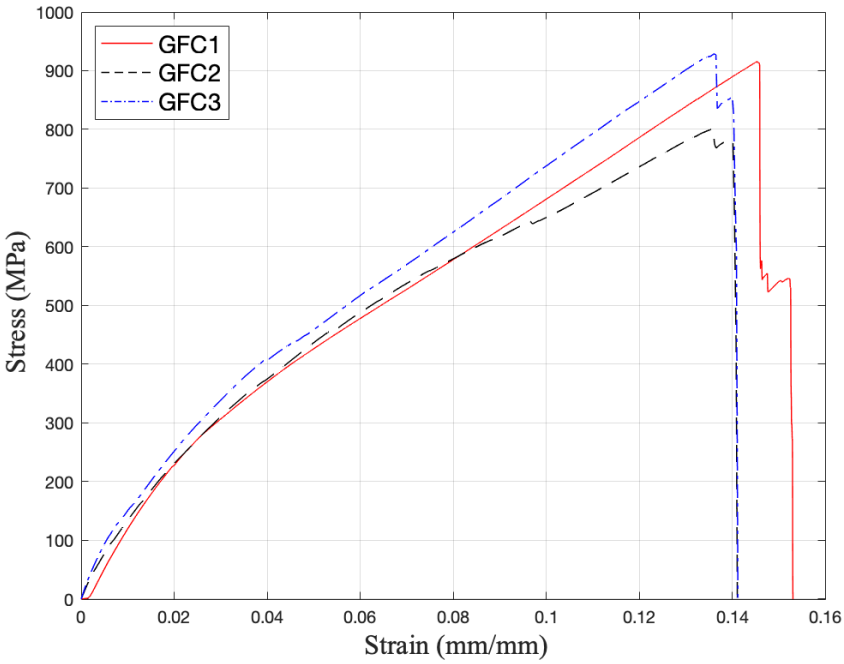

Figure 22. Glass fiber composites under tension until failure.

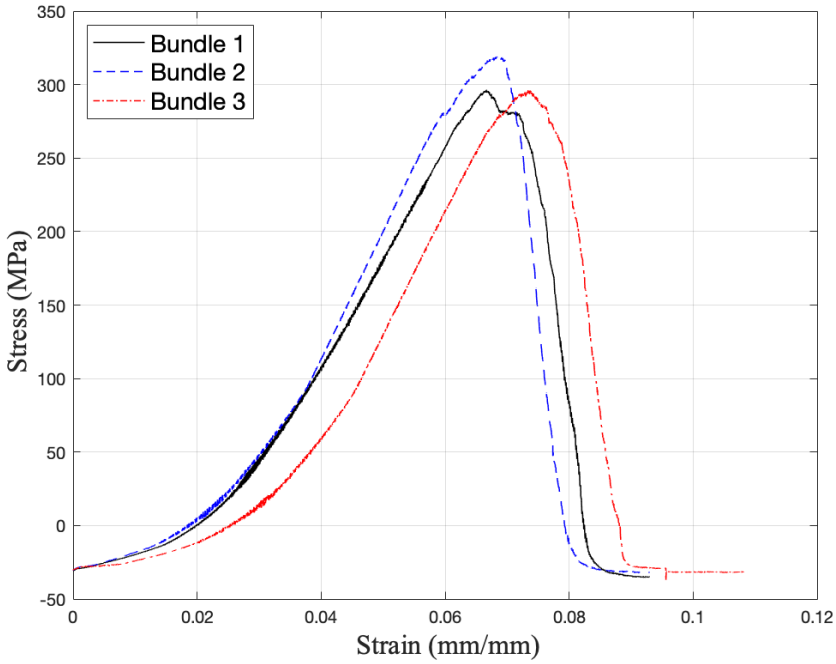

Figure 23. Glass fiber bundles under tension until failure.

2. Cyclic Loading

Similar to the tensile test results, cyclic loading until failure for GFC and GFB was consistent for both specimen types. The sudden failure behavior for GFC and gradual decrease in residual strength for GFB under tensile loading carried over to cyclic loading. A representation of the GFB's typical results is shown in Figure 24. Here, horizontal red lines were placed at the upper and lower limits of the GFB cyclic loading result to show how the dry fiber bundle's stress amplitude tapers down before complete failure. The reduction in stress of the GFB can be directly correlated to the failure of individual fibers during cyclic loading, resulting from slack fibers and uneven stress distribution. A physical progression of failure for the GFB is shown in Figure 25, where complete separation of all fibers does not dictate failure but when the bundle can no longer carry a load.

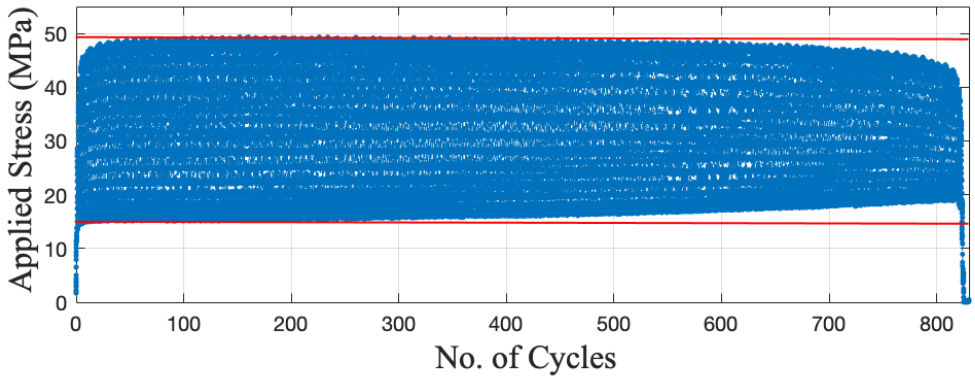

Figure 24. Typical results for GFB reflect a reduction in stress amplitude prior to failure.

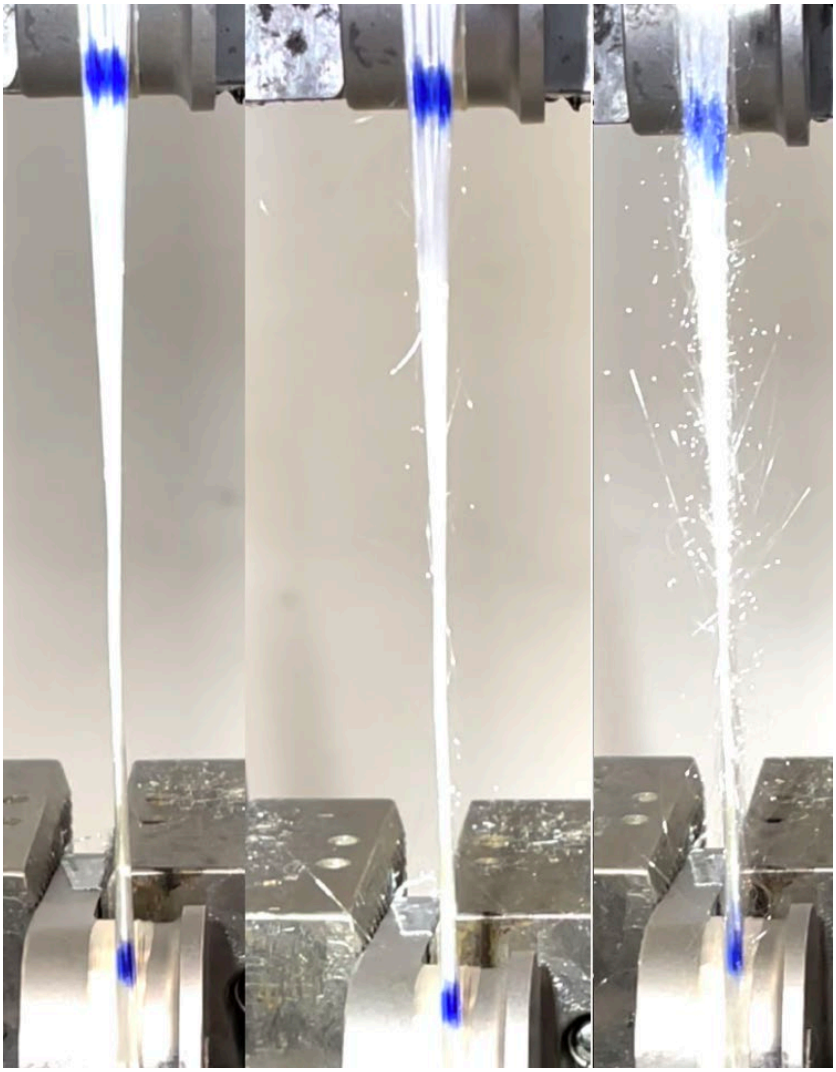

Figure 25. GFB preload (left), as fibers begin to break (middle), and after complete failure (right).

In the case of GFC, a representation of the typical results for cyclic loading until failure is shown in Figure 26. Here, specimen 16 failed suddenly and without warning. In Figure 27, specimen 16 is zoomed in at the failure location to show how abruptly the GFC failed. Unlike the GFB, as the fibers and or matrix fail in the composite, there is no significant change in the stress amplitude. This suggests, the GFC maintained the majority of its strength up until failure, just as it did under tensile testing. In addition, failure of individual fibers does not seem to be an issue as seen with the GFB, as the fibers are held together as one unit within the matrix.

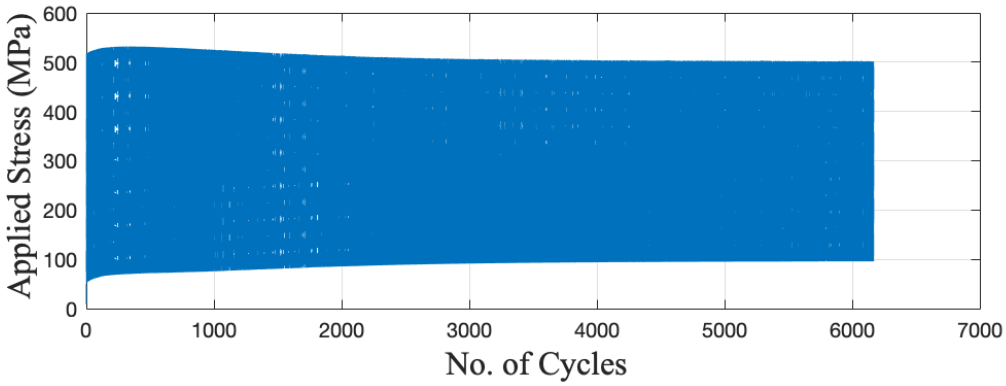

Figure 26. Representation of the typical results for GFC failure under cyclic load.

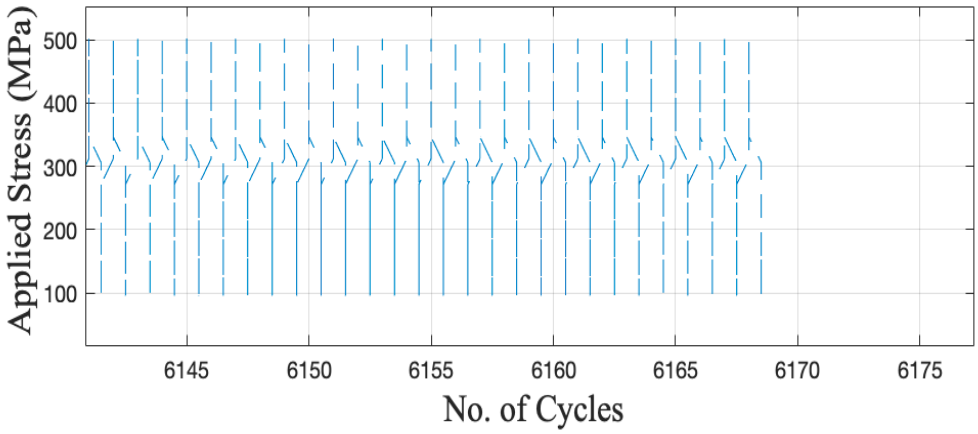

Figure 27. A close-up view of the sudden failure in GFC specimen 16.

Finally, the cyclic loading results until failure at the specified intervals described in Chapter 3, Tables 1 and 2, are given. Figures 28 and 29 show S-N curves for GFC and GFB; both show to be linear in failure when plotted as a function of force or stress.

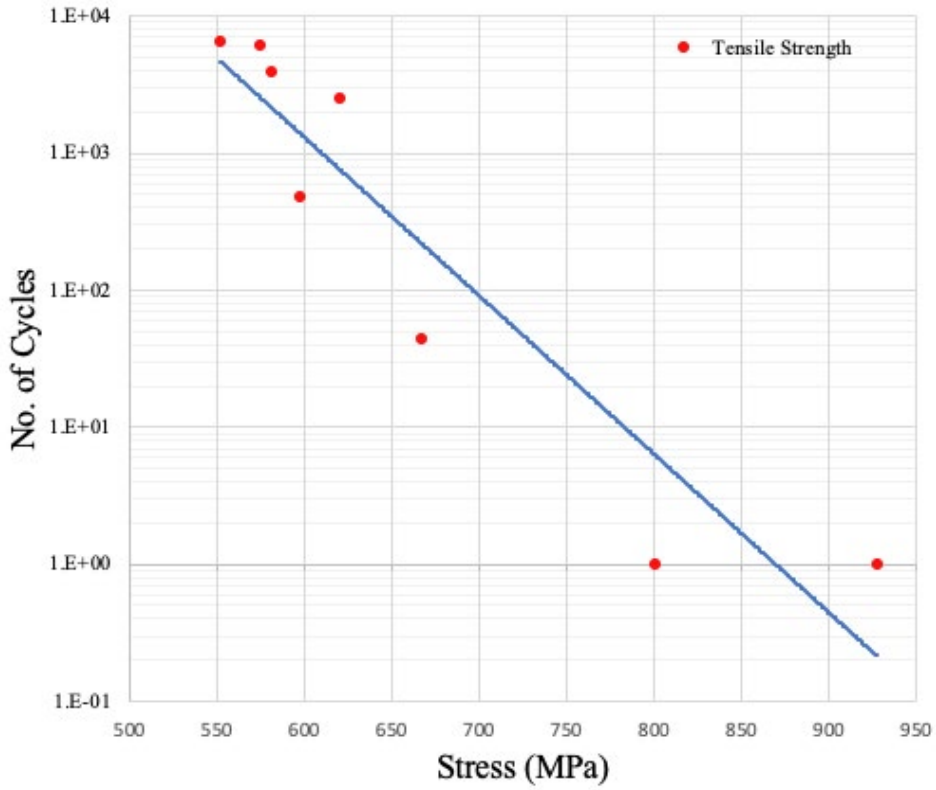

Figure 28. S-N Curve for glass fiber composites.

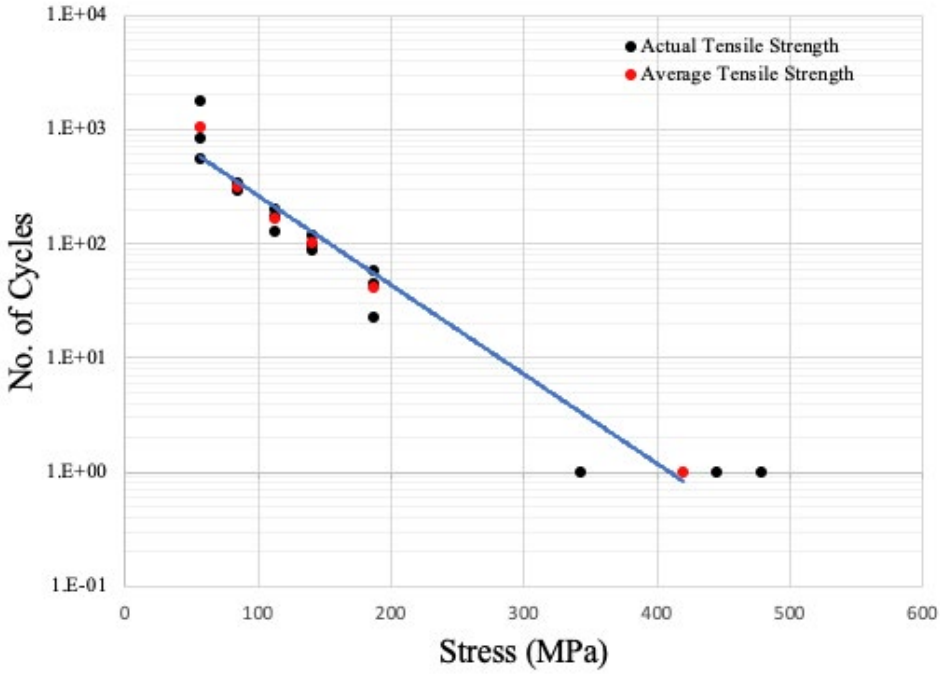

Figure 29. S-N Curve for dry glass fiber bundles.

3. Tensile Test Post-Cyclic Loading

The residual strength post cyclic loading was modeled with the probability of failure shown in equation (7), where $\sigma = \frac{\sigma_o}{f_i}$, and δ is a constant. Failure after (i+1) cycles is expressed in equation (8), where $\sigma_i = \frac{\sigma_o}{f_i}$ and the residual strength after n cycles is $f_n\sigma_f$. Assuming a δ value of 0.04896, the predicted residual strength of the GFC lined up well with the experimental data, as seen in Figure 30. This same model can be used to determine the residual strength of a GFB with a different δ value.

$$p(\sigma) = \begin{cases} \frac{\sigma}{\sigma_f} e^{-\delta\left(\frac{\sigma_f}{\sigma}-1\right)} & 0 \le \sigma \le \sigma_f \\ 1 & \sigma > \sigma_f \end{cases} \tag{7}$$

$$f_{i+1} = (1 - p(\sigma_i))f_i \tag{8}$$

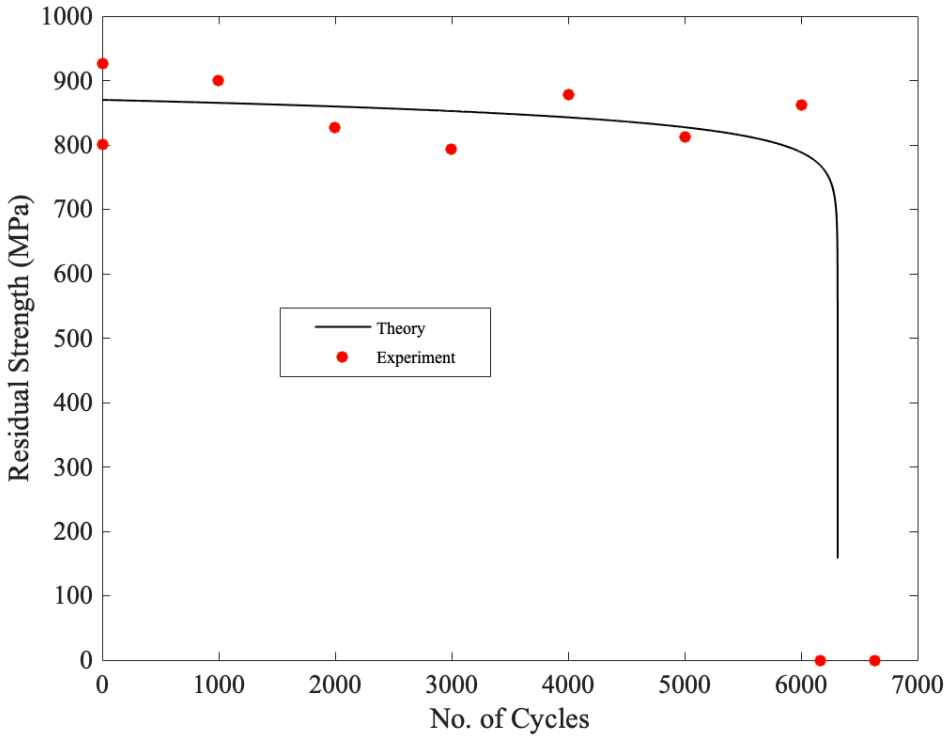

Figure 30. Glass fiber composite residual strength after cyclic loading.

B. FAILURE ANALYSIS OF NOTCHED MATERIAL

1. Tensile Test

As previously mentioned, tensile tests were conducted until failure for all PMMA and CFC QI specimens to examine the failure location for various notch geometries. The failure strength and behavior for PMMA specimen groups were consistent and showed little to no variation in their respective stress slope. A representation of PMMA's behavior is shown in Figure 31, with the ultimate tensile strength for all PMMA notch types shown in Figure 32. As expected, the ultimate tensile strength for the different notch types is proportional to the cross-section area where the failure occurred. Therefore, a decrease in the cross-section area leads to a decrease in the ultimate tensile strength. Pictures of each notch type before and after tensile testing are shown in Figure 33 for all PMMA specimens.

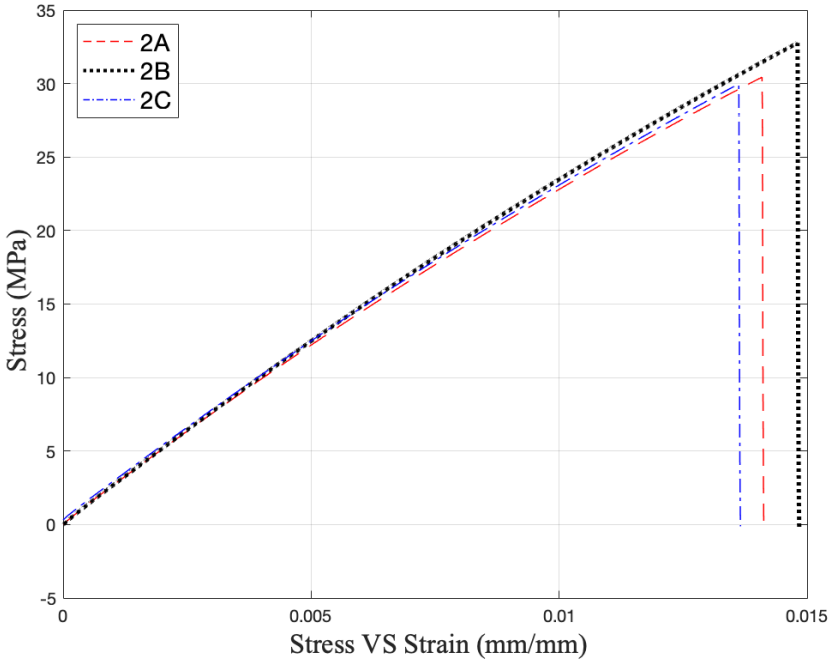

Figure 31. Representation of PMMA's failure behavior.

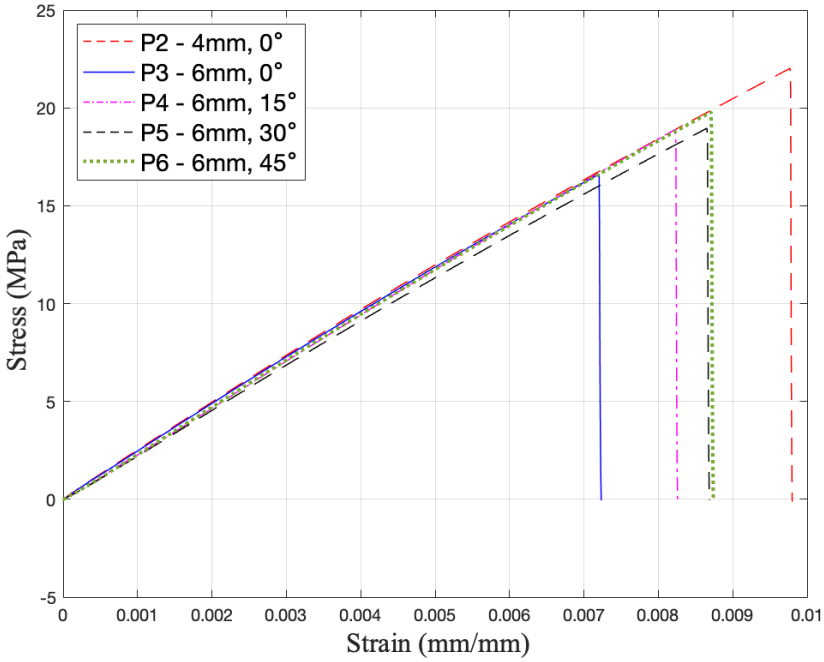

Figure 32. Comparison of all PMMA notched specimen.

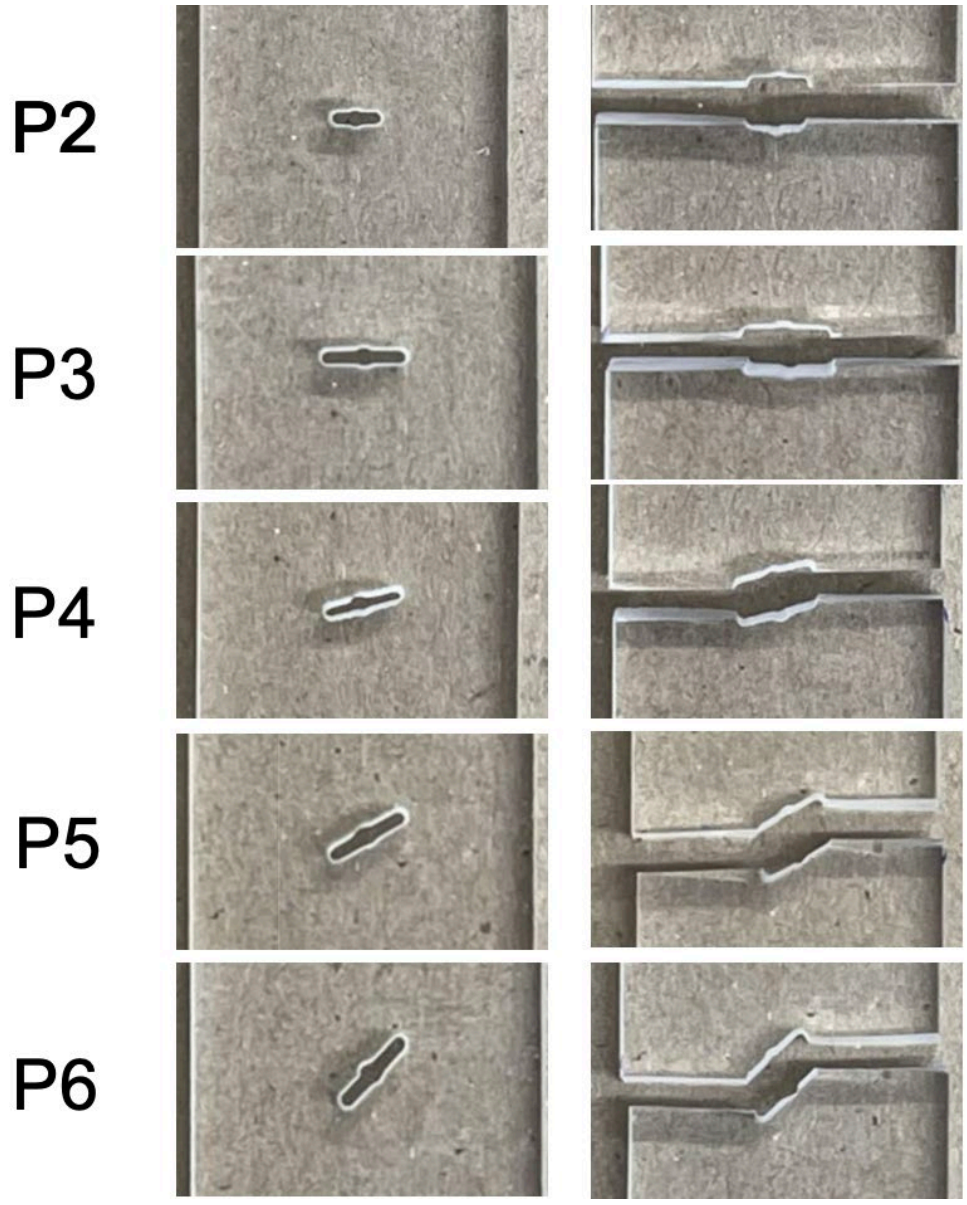

Figure 33. PMMA specimen notch types; before and after failure.

Similarly, failure strength and behavior for CFC QI specimen groups were consistent for all tensile tests. A representation of CFC QI behavior under tensile stress is seen in Figure 34, with the ultimate tensile strength for all CFC QI notch types shown in Figure 35. Failure in the CFC QI specimens was also proportional to the cross-sectional area where the failure occurred, as seen with the PMMA specimens. Pictures of each notch type before and after tensile testing are shown in Figure 36 for all CFC QI specimens.

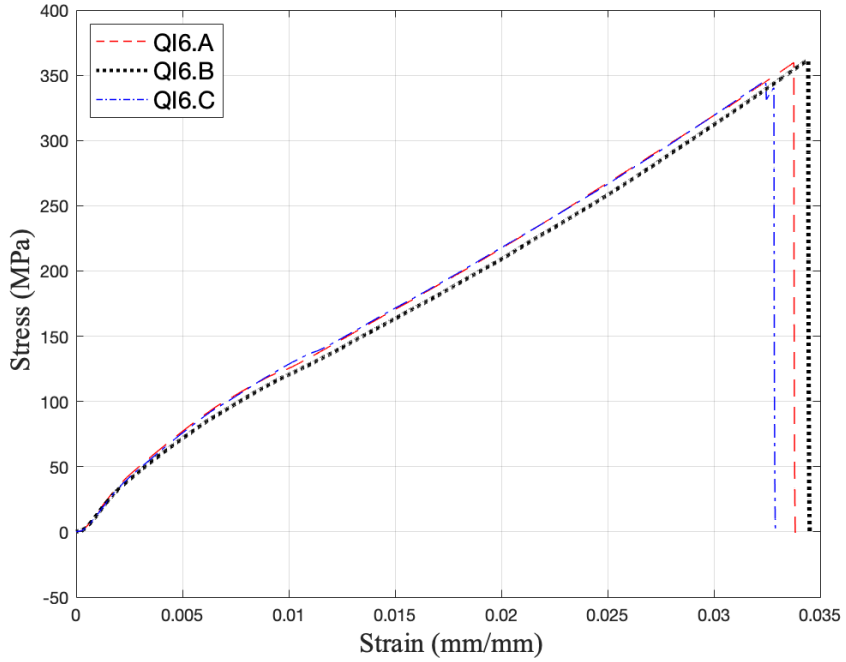

Figure 34. Representation of CFC QI failure behavior.

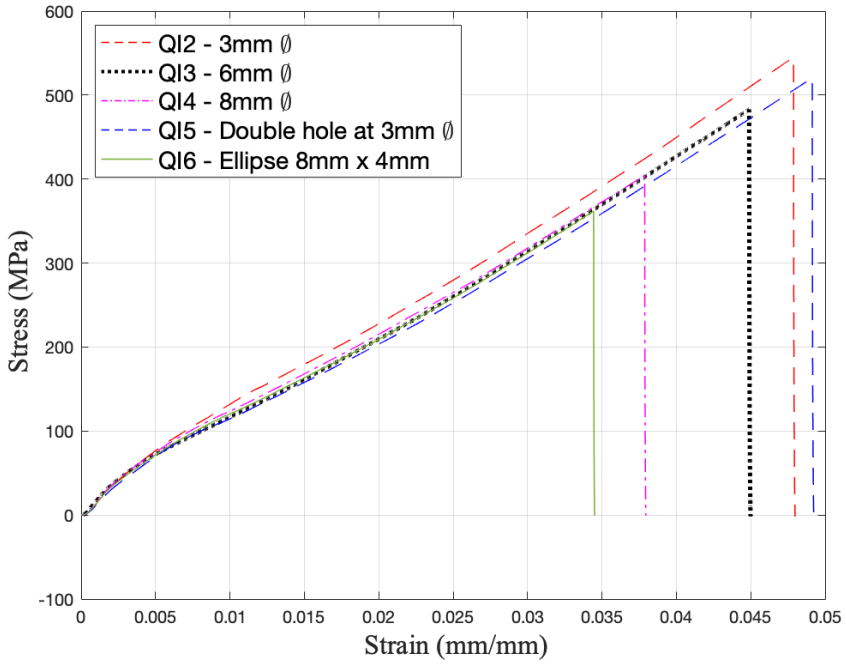

Figure 35. Comparison of all CFC QI notched specimens' tensile strengths.

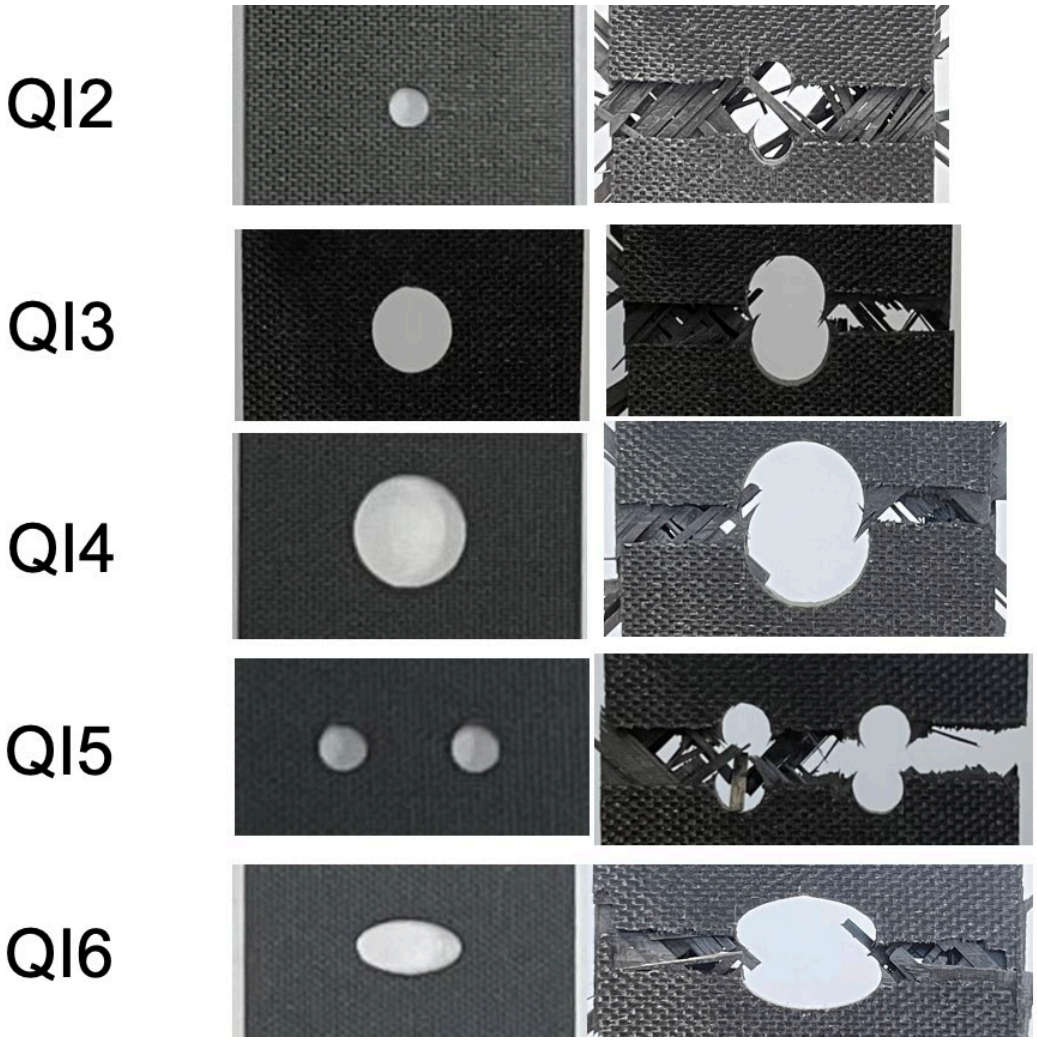

Figure 36. CFC QI specimen notch types; before and after failure.

2. Theory versus Experiment

The theoretical notched failure value, κ_{fail}, from equation (2) was determined with one of each tensile test result for PMMA, CFC QI, and CFC CP specimens with a notch. This theoretical failure value was then used to compare against the experimental failure for all specimens and notch variations.

Figures 37 through 38 reflect the results of this comparison for PMMA and CFC QI specimens, respectively. A previous student provided experimental data for CFC CP to compare against the theory and is shown in Figure 40. The reflected failure stress is the

average stress at the displacement location, as shown in Figure 17 for the quarter and 18 for full-size models.

Failure for all models occurred through the cross-section perpendicular to the loading direction for all notch types. In the finite element model, failure began at the notch location where stress was the highest and followed a path with the least stress gradient. Both criteria outlined in equations (1) and (2) were satisfied, thus proving the proposed failure criteria.

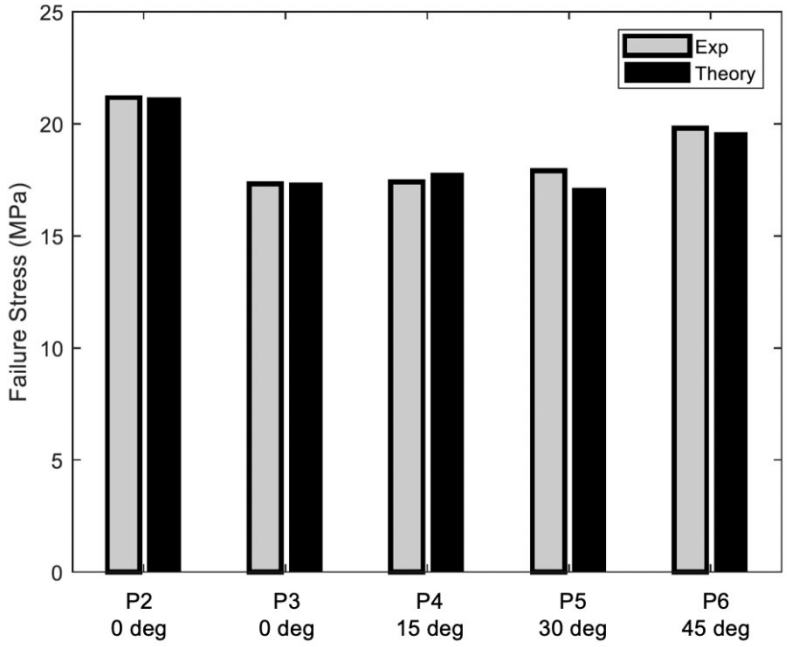

Figure 37. Experimental results for PMMA vs. the developed universal failure criteria.

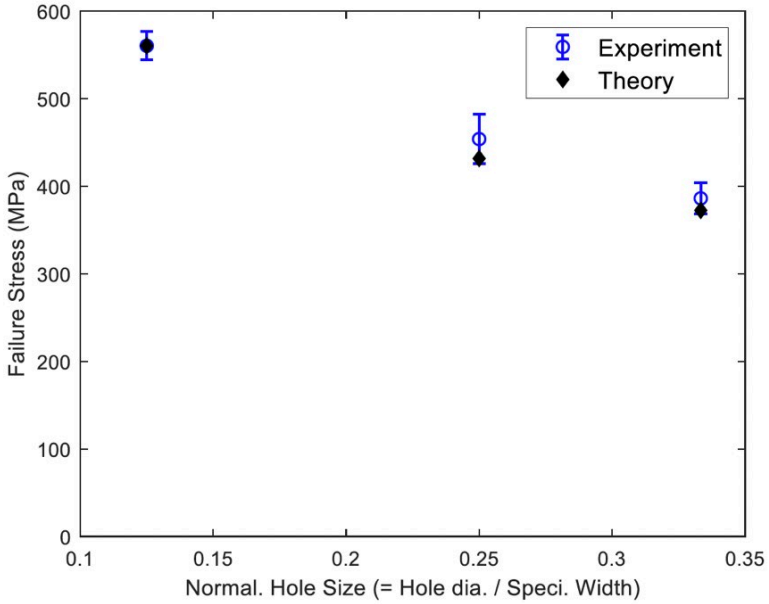

Figure 38. Experimental results for CFC-QI specimens with circular holes vs. the developed universal failure criteria.

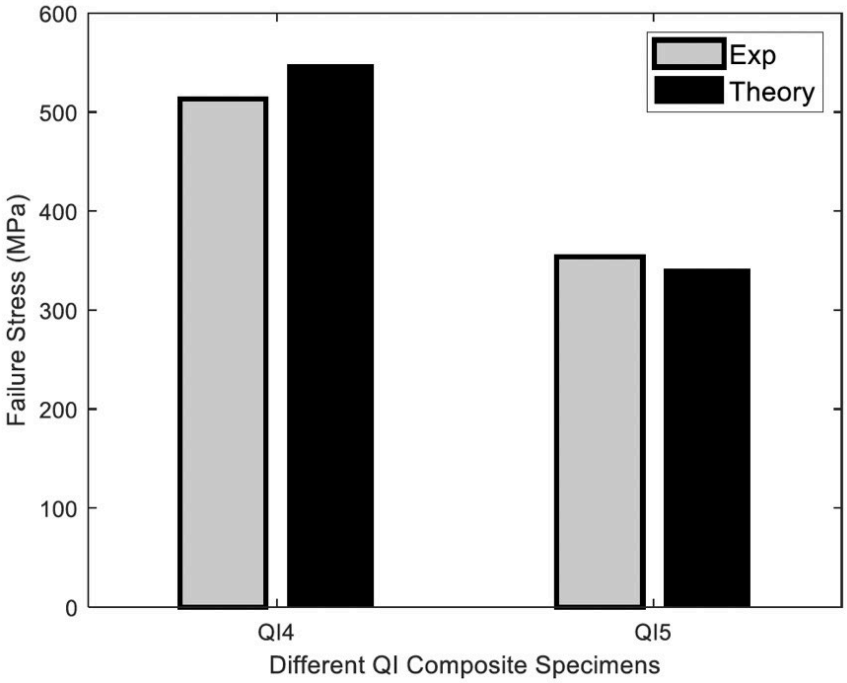

Figure 39. Experimental results for CFC-QI ellipse and double hole specimens vs. the developed universal failure criteria.

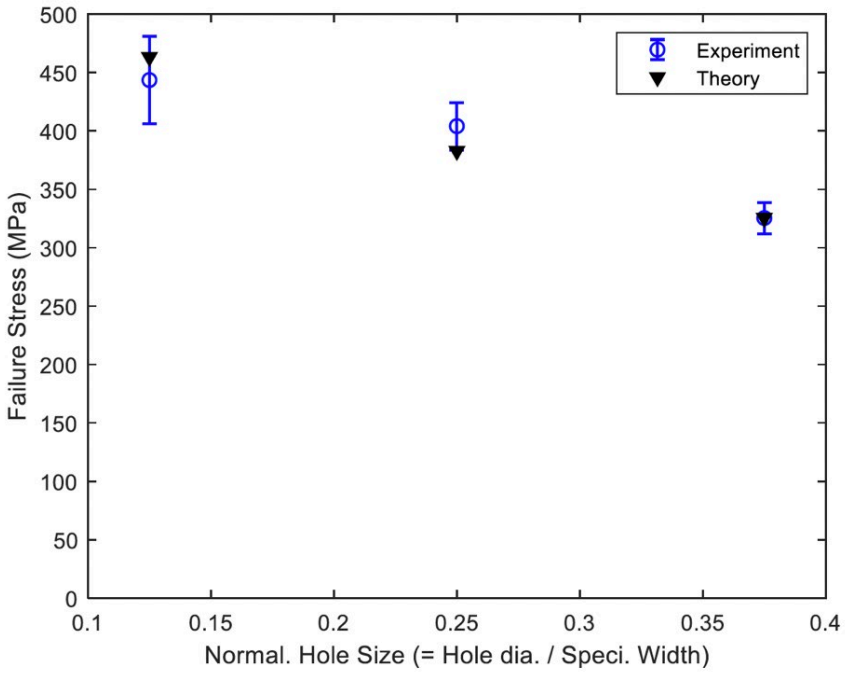

Figure 40. Experimental results for CFC-CP specimens with circular holes vs. the developed universal failure criteria.

THIS PAGE INTENTIONALLY LEFT BLANK

VI. CONCLUSION AND RECOMMENDATIONS

A. CONCLUSION

The objectives of this research were to accurately predict the residual strength of a glass fiber composite after cyclic loading for any number of cycles, create an S-N curve for glass fiber composites and glass fiber bundles, and assess the validity of universal failure criteria for notched specimens. First, the behavior and residual strength of a glass fiber composite after cyclic loading were examined using a multiscale approach. Next, the glass fiber composite's behavior was analyzed and compared to dry glass fiber bundles. Finally, a probabilistic model for residual strength after cyclic loading was created and compared against the experimental data. The S-N curves were created for glass fiber composites and bundles, and despite testing limitations, experimental data for the glass fiber composites agreed well with the probabilistic model.

The last objective was to validate the universal failure criteria for a notched specimen. Three different materials with various notch shapes were tensile tested to failure and analyzed using a FEM model. The tensile test provided the specimens' material properties, and the FEM model provided the theoretical notched failure value, κ_{fail}. Then, the proposed theory was compared to experimental results and proved, failure location and direction can be predicted accurately for multiple brittle materials regardless of their notch type.

B. LIMITATIONS AND RECOMMENDATIONS

1. Limitation of This Research

As a result of equipment inoperability, further data for residual strength was unavailable to be obtained for dry fiber bundles. In addition, even though residual strength after cyclic loading was found for glass fiber composites, additional tests at various loads would increase the model's accuracy and further validate the model.

2. Recommendations

- More residual strength after cyclic loading test should be conducted for glass fiber composites and dry fiber bundles to validate the proposed mathematical model further. After the model is validated, recommend testing against composites with perpendicular fiber orientations before moving to a more complex glass fiber composite.
- Create additional off-centered notch shapes that have not been tested and test against the universal failure criteria to confirm the theory holds regardless of notch location.
- Expand the universal failure criteria to multiaxial loading.

LIST OF REFERENCES

[1] Seracino, R., 2004, "FRP composites in civil engineering," in International Institute Conference Proceeding for FRP in Construction, Adelaide.

[2] Bajpai, R. P, Chandrasekhar, U., and Arankalle, A. 2014. *Innovative Design, Analysis, and Development Practices in Aerospace and Automotive Engineering*. New York: Springer.

[3] Haller, C. 2020. Study of Fatigue Failure of Composite Materials. Monterey: Calhoun.

[4] Zangenberg, J., Brondsted, P., and Gillespie Jr., JW. 2014. "Fatigue damage propagation in unidirectional glass fibre reinforced composites made of a non-crimp fabric." *Journal of Composite Materials* 48 (22): 2711–2727.

[5] Kwon, Y W. 2020, "Revisiting failure of brittle materials," *Journal of Pressure Vessel Technology*, Vol. 143, December, 064503.

[6] Callister Jr., W. D., and Rethwisch, D. G. 2010. *Materials Science and Engineering An Introduction*, John Wiley & Sons, NY.

[7] Vassilopoulos, A. P. 2020. *Fatigue Life Prediction of Composites and Composite Structures*. Cambridge: Elsevier.

[8] Suresh, S. 1998. *Fatigue of Materials*. Cambridge: University Press.

[9] Broek, D. 1986. *Elementary Engineering Fracture Mechanics*. Hingham: Kluwer Academic Publishers.

[10] Chou, P C, and R Croman. 1978. "Residual strength in fatigue based on the strength-life equal rank assumption." *Journal of Composite Materials* 177–194.

[11] Philippidis, T.P. and Passipoularidis, V.A. 2007. "Residual Strength after fatigue in composites: Theory vs. experiment." *International Journal of Fatigue* 29: 2104–2116.

[12] Khan, A. I., Venkataraman, S., and Miller, I. 2018. "Predicting Fatigue Damage of Composites Using Strength Degradation and Cumulative Damage Model." *Journal of Composites Science* 2 (9).

[13] A. Lakshminarayana, R Vijayakumar, and Krishnamohana, R. 2016. "Progressive failure analysis of laminated composite plates with elliptical or circular cutout using finite element method." *IOP Conf. Series: Materials Science and Engineering 149.* IOP Publishing.

[14] Deveci, H A, and Artem, H. S. 2018. “On the estimation and optimization capabilities of the fatigue life prediction models in composite laminates.” *Journal of Reinforced Plastic & Composites* 37 (21): 1304–1321.

[15] Kim, Ho Sung, and Saijie Huang. 2021. “S-N Curve Characterisation for Composite Materials and Prediction of Remaining Fatigue Life Using Damage Function.” *Journal of Composites Science* (MDPI) 5 (76).

[16] D’Amore, Albert, Giorgio, Massimiliano, Grassia, Luigi. 2015. “Modeling the residual strength of carbon fiber reinforced composites subjected to cyclic loading.” *International Journal of Fatigue* 78: 31–37.

[17] Salviato, M, Kirane, K, Bazant, Z P. 2013. “Statistical distribution and size effect of residual strength of quasi-brittle materials after a period of constant load.” *Journal of the Mechanics and Physics of Solids* 64: 440–454.

[18] C. Srilakshmi, G. Sambasivarao and J. Suresh Kumar, “A review on Progressive failure analysis of composites,” 2021 *IOP Conf. Series: Material Science and Engineering,* vol. 01, no. 1185, 2020.

[19] X. F. Xu, Multiscale Theory of Composites and Random Media, Boca Raton: Taylor & Francis Group, 2019.

[20] Tay, T E, G Liu, V B Tan, X S Sun, and D C Pham. 2008. “Progressive Failure Analysis of Composites.” *Journal of Composite Materials* 1921–1966.

[21] Okayasu, Mitsuhiro, Tomohiro Yamazaki, Kohei Ota, Keiji Ogi, and Tetsuro Shiraishi. 2013. “Mechanical properties and failure characteristics of a recycled CFRP under tensile and cyclic loading.” *International Journal of Fatigue* 257–267.

[22] Zangenberg, Jens, Povl Brondsted, and John W Gillespie Jr. 2014. “Fatigue damage propagation in unidirectional glass fibre reinforced composites made of a non-crimp fabric.” *Journal of Composite Materials* 48 (22): 2711–2727.

[23] Hosseiny, Seyed, and Johnny Jakobsen. 2018. “Fatigue damage simulation of tension-tension loaded glass/polyester fiber composites with thickness tapering effects.” *Journal of Composite Materials* (SAGE) 53 (3): 297–314.

[24] Sorensen, Bent F. 2018. “The critical damage state controlling the tension-tension fatigue life of unidirectional fibre composites.” *Composites Science and Technology* (Elsevier Ltd).

[25] Swolfs, Yentl, Robert M McMeeking, Ignaas Verpoest, and Larissa Gorbatikh. 2015. “Matix cracks around fibre breaks and their effect on stress redistribution and failure development in unidirectional composites.” *Composites Science and Technology.*

[26] Yongbo, Z, F Huimin, W Zhihua, and M Xiaobing. 2015. “Open hole fatigue characteristic and probabilistic model for fatigue life prediction of CCF300/ QY89II and T300/QY89II composite laminates.” *Journal of Composite Materials* 3205–3214.

[27] Kadlec, L, Y W Kwon, C Haller, C M Park, and J M Didoszak. 2021. “Tensile and cyclic loading of fiber bundles.” *Multiscale and Multidisciplinary Modeling, Experiments and Design* 245–257.

[28] Ha, Sung Kyu, Chao Zhao, and Matthias De Monte. 2018. “Progressive failure prediction of short fiber reinforced composites using a multiscale approach.” *Journal of Composite Materials* (SAGE) 52 (27): 3785–3801.

[29] Kwon, Y W, and J Darcy. 2017. “Failure criteria for fibrous composites based on multiscale modeling.” *Multiscale and Multidisp. Model. Exp. And Des.* 3–17.

[30] Texonic. n.d. *Standard Product Selection.* Accessed September 18, 2021. https://texonic.net/en/tableau/standard-product-selection/#glass.

[31] INSTRON. n.d. *5980 Series Universal Testing System.* Accessed September 23, 2021. https://www.instron.com/en-us/products/testing-systems/universal-testing-systems/high-force-universal-testing-systems/5980-series-floor-models?region=North%20America.

[32] MTS Systems Corporation. n.d. *MTS 810 & 858 Material Testing Systems.* Accessed September 23, 2021. https://www.upc.edu/sct/documents_equipament/d_77_id-412.pdf.

[33] Ansys 2021 R1, User Manual, Ansys Inc.

THIS PAGE INTENTIONALLY LEFT BLANK

INITIAL DISTRIBUTION LIST

1. Defense Technical Information Center
   Ft. Belvoir, Virginia

2. Dudley Knox Library
   Naval Postgraduate School
   Monterey, California